DISCRETE AND CONTINUOUS
DYNAMICAL SYSTEMS SERIES S
Volume **8**, Number **3**, June **2015**

doi:10.3934/dcdss.2015.8.389

pp. **389–417**

DETECTION, RECONSTRUCTION, AND CHARACTERIZATION ALGORITHMS FROM NOISY DATA IN MULTISTATIC WAVE IMAGING

Habib Ammari

Department of Mathematics and Applications
Ecole Normale Supérieure
45 Rue d'Ulm, 75005 Paris, France

Josselin Garnier

Laboratoire de Probabilités et Modèles Aléatoires
& Laboratoire Jacques-Louis Lions
Université Paris Diderot
75205 Paris Cedex 13, France

Vincent Jugnon

Department of Mathematics
Massachusetts Institute of Technology
77 Massachusetts Avenue, Cambridge, MA 02139-4307, USA

Abstract. The detection, localization, and characterization of a collection of targets embedded in a medium is an important problem in multistatic wave imaging. The responses between each pair of source and receiver are collected and assembled in the form of a response matrix, known as the multi-static response matrix. When the data are corrupted by measurement or instrument noise, the structure of the response matrix is studied by using random matrix theory. It is shown how the targets can be efficiently detected, localized and characterized. Both the case of a collection of point reflectors in which the singular vectors have all the same form and the case of small-volume electromagnetic inclusions in which the singular vectors may have different forms depending on their magnetic or dielectric type are addressed.

1. **Introduction.** The principle of imaging with waves is to use waves in order to probe an unknown medium. These waves can be acoustic, elastic, optic, or electromagnetic. They are emitted by a set of sources and they are recorded by a set of sensors (transducers in acoustics, seismographs in geophysics, antennas in electromagnetics, etc). Multistatic imaging usually has two steps. The first step consists in collecting the waves generated by the sources and recorded by the receivers. The data set consists of a matrix of recorded signals, known as the multistatic response matrix, whose indices are the index of the source and the index of the receiver. The second step consists in processing the recorded data in order to estimate some relevant features of the medium (reflector locations,...); see, for instance, [36].

2010 *Mathematics Subject Classification.* Primary: 78M35, 78A46; Secondary: 15B52.

Key words and phrases. Multistatic wave imaging, noisy data, detection and reconstruction algorithms, random matrices, measurement noise, Helmholtz equation.

This work was supported by the ERC Advanced Grant Project MULTIMOD–267184.

The main applications that we have in mind are medical imaging (such as microwave and electrical impedance breast cancer detections), airport security screening, geophysical exploration, and non-destructive testing; see, for instance, [1, 24, 43]. For such applications, the general purpose of multistatic imaging is, from imperfect information (rough forward models, limited and noisy data), to estimate parts of the unknown structure that is of interest.

In this paper we consider, in the presence of noise, the detection and localization of point reflectors and small-volume inclusions embedded in a medium by probing the medium with time-harmonic scalar waves emitted from and recorded on a sensor array. The data are assumed to be corrupted by instrument noise. We are also interested in characterizing the physical nature of the inclusions. We use random matrix theory tools to study these problems in the presence of measurement noise. The measurement noise can be modeled by an additive complex Gaussian matrix with zero mean.

Our first goal in this work is to design an efficient procedure for detecting point reflectors. For doing so, we relate the eigenvalues of the measured response matrix to those of the response matrix in the absence of any noise and give their statistical distributions (Theorem 2.1). For given false alarm rate, we provide an estimation of the number of reflectors and propose an imaging functional to locate them. We also estimate their physical parameters. Our second goal is to extend the obtained results and proposed algorithms developed in the case of point reflectors to the case of small-volume inclusions. In contrast to the case of point reflectors, the eigenvectors associated with the response matrix do not have the same form. Exploiting this observation, we show that the statistical distributions of the angles between the left and the right singular vectors of the response matrix (Theorem 3.1) allow us not only to detect a collection of small-volume inclusions but also to characterize their nature. We also design two location estimators. The second one is a refinement of the first. Numerical illustrations to highlight the potential of proposed detection, reconstruction, and characterization algorithms are presented. For the sake of simplicity, we only consider the two-dimensional case. Similar results can be easily derived in three dimensions.

Throughout this paper, we only consider the full-view case, where the sensor arrays englobe the reflectors and the inclusions to be imaged. It turns out that the generalization of the analytical formulas obtained in this paper to the limited-view case is quite involved, see [8]. We refer the reader to [6, 9, 16] for related works on multistatic imaging.

2. Detection of point reflectors.

2.1. Problem formulation.

Let us consider the propagation of scalar waves in $\mathbb{R}^2$. In the presence of r localized reflectors the speed of propagation can be modeled by

$$\frac{1}{c^2(\boldsymbol{x})} = \frac{1}{c_0^2}\Big(1 + \sum_{j=1}^{r} V_j(\boldsymbol{x})\Big). \tag{1}$$

Here

- the constant c_0 is the known background speed,
- the local variation $V_j(\boldsymbol{x})$ of the speed of propagation induced by the reflector at $\boldsymbol{x}_j$ is

$$V_j(\boldsymbol{x}) = \eta_j \mathbf{1}_{\Omega_j}(\boldsymbol{x} - \boldsymbol{x}_j), \tag{2}$$

where Ω_j is a compactly supported domain with volume l_j^2, $\mathbf{1}_{\Omega_j}$ is the characteristic function of Ω_j, and η_j is the dielectric contrast (or the strength of the point reflector at $\boldsymbol{x}_j$).

Suppose that a time-harmonic point source acts at the point $\boldsymbol{z}$ with frequency ω. The field in the presence of the reflectors is the solution $\hat{u}(\cdot, \boldsymbol{z})$ to the following transmission problem:

$$\Delta_{\boldsymbol{x}} \hat{u} + \frac{\omega^2}{c^2(\boldsymbol{x})} \hat{u} = -\delta_{\boldsymbol{z}}(\boldsymbol{x}), \tag{3}$$

with the radiation condition imposed on $\hat{u}$.

Suppose that we have a transmitter array of M sources located at $\{\boldsymbol{z}_1, \ldots, \boldsymbol{z}_M\}$ and a receiver array of N elements located at $\{\boldsymbol{y}_1, \ldots, \boldsymbol{y}_N\}$. The $N \times M$ response matrix $\mathbf{A}$ describes the transmit-receive process performed at these arrays. The field received by the nth receiving element $\boldsymbol{y}_n$ when the wave is emitted from $\boldsymbol{z}_m$ is $\hat{u}(\boldsymbol{y}_n, \boldsymbol{z}_m)$. If we remove the incident field then we obtain the (n, m)-th entry of the response matrix:

$$A_{nm} = \hat{u}(\boldsymbol{y}_n, \boldsymbol{z}_m) - \hat{G}(\omega, \boldsymbol{y}_n, \boldsymbol{z}_m). \tag{4}$$

The incident field is the homogeneous Green's function $\hat{G}(\omega, \boldsymbol{x}, \boldsymbol{y})$ of the wave equation. It is given by

$$\hat{G}(\omega, \boldsymbol{x}, \boldsymbol{y}) = \frac{i}{4} H_0^{(1)}\Big(\frac{\omega}{c_0}|\boldsymbol{y} - \boldsymbol{x}|\Big), \tag{5}$$

in a two-dimensional medium. Here $H_0^{(1)}$ is the zeroth order Hankel function of the first kind.

Finally, taking into account measurement noise, the measured response matrix $\mathbf{B}$ is

$$\mathbf{B} = \mathbf{A} + \frac{1}{\sqrt{M}} \mathbf{W}, \tag{6}$$

where the matrix $\mathbf{W}$ represents the additive measurement noise, which is a random matrix with independent and identically distributed complex entries with Gaussian statistics, mean zero and variance σ_{noise}^2. We assume here

Assumption 1. $\eta_j l_j^3 \ll \frac{1}{\sqrt{M}} \sigma_{\text{noise}}$.

Assumption 1 insures that indeed the instrument errors dominate the remainder in the Born approximation.

Moreover, the particular scaling for the noise level is the right one to get nontrivial asymptotic regimes in the limit $M \to \infty$. Furthermore, it is the regime that emerges from the use of the Hadamard acquisition scheme for the response matrix. Hadamard's technique allows us to acquire simultaneously the elements of the MSR matrix and to reduce the noise level. It uses the structure of Hadamard matrices. Its feature is to divide the variance of the noise by the number of sources [4, 30].

The goal is to estimate the number of reflectors, their positions and their material properties from the measured response matrix $\mathbf{B}$.

2.2. **Singular value decomposition of the response matrix.** In the Born approximation, where the volume of $\Omega_j, j = 1, \ldots, r$, goes to zero, the measured field has approximately the form

$$\hat{u}(\boldsymbol{y}_n, \boldsymbol{z}_m) = \hat{G}(\omega, \boldsymbol{y}_n, \boldsymbol{z}_m) + \sum_{j=1}^{r} \rho_j \hat{G}(\omega, \boldsymbol{y}_n, \boldsymbol{x}_j) \hat{G}(\omega, \boldsymbol{x}_j, \boldsymbol{z}_m), \tag{7}$$

for $n = 1, \dots, N$, $m = 1, \dots, M$, where ρ_j is the coefficient of reflection defined by

$$\rho_j = \frac{\omega^2}{c_0^2} \eta_j l_j^2 \tag{8}$$

(recall that η_j is the dielectric contrast and l_j^2 is the physical volume of the j-th reflector). We introduce the normalized vector of Green's functions from the receiver array to the point $\boldsymbol{x}$:

$$\boldsymbol{u}(\boldsymbol{x}) := \frac{1}{\big(\sum_{l=1}^N |\hat{G}(\omega, \boldsymbol{x}, \boldsymbol{y}_l)|^2\big)^{\frac{1}{2}}} \big(\hat{G}(\omega, \boldsymbol{x}, \boldsymbol{y}_n)\big)_{n=1,\dots,N}, \tag{9}$$

and the normalized vector of Green's functions from the transmitter array to the point $\boldsymbol{x}$, known as the illumination vector, as follows:

$$\boldsymbol{v}(\boldsymbol{x}) := \frac{1}{\big(\sum_{l=1}^M |\hat{G}(\omega, \boldsymbol{x}, \boldsymbol{z}_l)|^2\big)^{\frac{1}{2}}} \big(\overline{\hat{G}(\omega, \boldsymbol{x}, \boldsymbol{z}_m)}\big)_{m=1,\dots,M}. \tag{10}$$

We can then write the response matrix in the form

$$\mathbf{A} = \sum_{j=1}^r \sigma_j \boldsymbol{u}(\boldsymbol{x}_j) \boldsymbol{v}(\boldsymbol{x}_j)^\dagger, \tag{11}$$

with

$$\sigma_j := \rho_j \Big(\sum_{n=1}^N |\hat{G}(\omega, \boldsymbol{x}_j, \boldsymbol{y}_n)|^2 \Big)^{\frac{1}{2}} \Big(\sum_{m=1}^M |\hat{G}(\omega, \boldsymbol{x}_j, \boldsymbol{z}_m)|^2 \Big)^{\frac{1}{2}}. \tag{12}$$

Here $\dagger$ denotes the conjugate transpose.

Throughout this paper, we assume that the arrays of transmitters and receivers are equi-distributed on a disk or a sphere englobing the point reflectors. Moreover, the point reflectors are at a distance from the arrays of transmitter and receivers much larger than the wavelength $2\pi c_0/\omega$. Provided that the positions $\boldsymbol{x}_j$ of the reflectors are far from one another (i.e., farther than the wavelength $2\pi c_0/\omega$), the vectors $\boldsymbol{u}(\boldsymbol{x}_j)$, $j = 1, \dots, r$, are approximately orthogonal to one another, as well as are the vectors $\boldsymbol{v}(\boldsymbol{x}_j)$, $j = 1, \dots, r$. In fact, from the Helmholtz-Kirchhoff theorem (see, for instance, [2]), we have

$$\frac{1}{N} \sum_{n=1}^N \hat{G}(\omega, \boldsymbol{x}_j, \boldsymbol{y}_n) \overline{\hat{G}(\omega, \boldsymbol{x}_i, \boldsymbol{y}_n)} \simeq \frac{c_0}{\omega} J_0\big(\frac{\omega}{c_0} |\boldsymbol{x}_i - \boldsymbol{x}_j|\big) \tag{13}$$

as $N \to +\infty$, where J_0 is the Bessel function of the first kind and of order zero. Moreover, $J_0(\frac{\omega}{c_0}|\boldsymbol{x}_i - \boldsymbol{x}_j|) \simeq 0$ when $|\boldsymbol{x}_j - \boldsymbol{x}_i|$ is much larger than the wavelength. The matrix $\mathbf{A}$ then has rank r and its non-zero singular values are σ_j, $j = 1, \dots, r$, with the associated left and right singular vectors $\boldsymbol{u}(\boldsymbol{x}_j)$ and $\boldsymbol{v}(\boldsymbol{x}_j)$.

The reconstruction algorithm that we introduce in the next section will make use of the following result proved in Appendix A.

Theorem 2.1. *Let $\mathbf{A}$ be an $N \times M$ deterministic matrix with rank r. Let us denote $\sigma_1(\mathbf{A}) \geq \cdots \geq \sigma_r(\mathbf{A}) > 0$ its nonzero singular values. Let $\mathbf{W}$ be an $N \times M$ random matrix with independent and identically distributed complex entries with Gaussian statistics, mean zero, and variance σ_{noise}^2. We define*

$$\mathbf{B} = \mathbf{A} + \frac{1}{\sqrt{M}} \mathbf{W}.$$

When $\gamma = N/M$ and r are fixed and $M \to \infty$, for any $j = 1, \dots, r$, we have

$$\sigma_j(\mathbf{B}) \overset{M\to\infty}{\longrightarrow} \begin{cases} \sigma_{\text{noise}}\Big(\dfrac{\sigma_j^2(\mathbf{A})}{\sigma_{\text{noise}}^2} + 1 + \gamma + \gamma\dfrac{\sigma_{\text{noise}}^2}{\sigma_j^2(\mathbf{A})}\Big)^{\frac{1}{2}} & \text{if } \sigma_j(\mathbf{A}) > \gamma^{\frac{1}{4}}\sigma_{\text{noise}}, \\ \sigma_{\text{noise}}(1+\gamma^{\frac{1}{2}}) & \text{if } \sigma_j(\mathbf{A}) \le \gamma^{\frac{1}{4}}\sigma_{\text{noise}} \end{cases} \tag{14}$$

in probability.

Theorem 2.1 shows how the singular values of the perturbed response matrix $\mathbf{B}$ are related to the singular values of the unperturbed response matrix $\mathbf{A}$. We can see that there is level repulsion for the singular values $\sigma_j(\mathbf{A})$ that are larger than the threshold value $\gamma^{1/4}\sigma_{\text{noise}}$, in the sense that $\sigma_j(\mathbf{B}) > \sigma_j(\mathbf{A})$. We can also observe that the singular values $\sigma_j(\mathbf{A})$ that are smaller than the threshold value $\gamma^{1/4}\sigma_{\text{noise}}$ are absorbed in the deformed quarter-circle distribution of the singular values of the noise matrix $\mathbf{W}/\sqrt{M}$.

2.3. **Algorithm for detection, localization, and reconstruction.** We denote $\gamma = N/M$. In the first version of the algorithm we assume that the noise level σ_{noise} is known. The algorithm is then the following one.

1. Compute the singular values $\sigma_j(\mathbf{B})$ of the measured response matrix.
2. Estimate the number of reflectors by

$$\hat{r} = \max\big\{j, \sigma_j(\mathbf{B}) > \sigma_{\text{noise}}\big(1+\gamma^{\frac{1}{2}} + r_\alpha\big)\big\},$$

where the threshold value

$$r_\alpha = \frac{1}{2M^{\frac{2}{3}}}\big(1+\gamma^{-\frac{1}{2}}\big)^{\frac{1}{3}}\Phi_{\text{TW2}}^{-1}(1-\alpha), \tag{15}$$

ensures that the false alarm rate (for the detection of a reflector) is α [7, 30]. Here Φ_{TW2} is the cumulative distribution function of the Tracy-Widom distribution of type 2 [10, 33]. Recall that the type-2 Tracy-Widom distribution has the probability distribution function $p_{\text{TW2}}(x)$ such that

$$\int_{-\infty}^{y} p_{\text{TW2}}(x)dx = \exp\Big(-\int_y^\infty (x-y)\varphi^2(x)dx\Big),$$

where φ is the solution of the Painlevé equation

$$\varphi''(x) = x\varphi(x) + 2\varphi(x)^3, \qquad \varphi(x) \overset{x\to+\infty}{\approx} \text{Ai}(x), \tag{16}$$

with Ai being the Airy function. The expectation is $\int x p_{\text{TW2}}(x)dx \approx -1.77$ and the variance is approximately 0.81. We have, for instance, $\Phi_{\text{TW2}}^{-1}(0.9) \simeq -0.60$, $\Phi_{\text{TW2}}^{-1}(0.95) \simeq -0.23$, and $\Phi_{\text{TW2}}^{-1}(0.99) \simeq 0.48$.

3. For each $j = 1, \dots, \hat{r}$, estimate the positions $\boldsymbol{x}_j$ of the jth reflector by looking after the position $\hat{\boldsymbol{x}}_j$ of the global maximum of the subspace imaging functional $\mathcal{I}_j(\boldsymbol{x})$ defined by

$$\mathcal{I}_j(\boldsymbol{x}) = \big|\boldsymbol{u}(\boldsymbol{x})^\dagger \boldsymbol{u}_j(\mathbf{B})\big|^2. \tag{17}$$

Here, $\boldsymbol{u}_j(\mathbf{B})$ is the j-th left singular vector of the measured response matrix $\mathbf{B}$ (i.e., the left singular vector associated to the j-th largest singular value) and $\boldsymbol{u}(\boldsymbol{x})$ is defined by (9). We use here the left singular vectors rather than the right ones because they correspond to the image (receiver) space and there are usually more receivers than transmitters ($N \ge M$).

4. For each $j = 1, \dots, \hat{r}$, estimate the amplitudes ρ_j of the j-th reflector by

$$\hat{\rho}_j = \Big(\sum_{n=1}^{N} |\hat{G}(\omega, \hat{\boldsymbol{x}}_j, \boldsymbol{y}_n)|^2 \Big)^{-\frac{1}{2}} \Big(\sum_{m=1}^{M} |\hat{G}(\omega, \hat{\boldsymbol{x}}_j, \boldsymbol{z}_m)|^2 \Big)^{-\frac{1}{2}} \hat{\sigma}_j, \tag{18}$$

with $\hat{\sigma}_j$ being the estimator of $\sigma_j(\mathbf{A})$ defined by

$$\hat{\sigma}_j = \frac{\sigma_{\rm noise}}{\sqrt{2}} \Big[\frac{\sigma_j^2(\mathbf{B})}{\sigma_{\rm noise}^2} - 1 - \gamma + \Big(\big(\frac{\sigma_j^2(\mathbf{B})}{\sigma_{\rm noise}^2} - 1 - \gamma \big)^2 - 4\gamma \Big)^{\frac{1}{2}} \Big]^{\frac{1}{2}}. \tag{19}$$

The form of the estimator $\hat{\sigma}_j$ comes from the inversion of relation (14). If we were using $\sigma_j(\mathbf{B})$ as an estimator of $\sigma_j(\mathbf{A})$, then we would over-estimate the coefficients of reflection of the reflectors.

Note that we do not need to compute all the singular values of the measured response matrix $\mathbf{B}$, only the singular values larger than $\sigma_{\rm noise}(1 + \gamma^{\frac{1}{2}})$ need to be computed.

If the noise level is not known, the first two steps of the algorithm must be replaced by the following ones:

1. Set $j = 1$ and define $\mathbf{B}_1 = \mathbf{B}$.
2. (a) Compute the largest singular value $\sigma_1(\mathbf{B}_j)$ (i.e., the spectral norm of $\mathbf{B}_j$) and the associated singular vectors $\boldsymbol{u}_1(\mathbf{B}_j)$ and $\boldsymbol{v}_1(\mathbf{B}_j)$.
   (b) Compute the Frobenius norm $\|\mathbf{B}_j\|_F$ and estimate the noise level by [7, 30]

$$\hat{\sigma}_{{\rm n},j} = \gamma^{-\frac{1}{2}} \left[\frac{\|\mathbf{B}_j\|_F^2 - \sigma_1^2(\mathbf{B}_j)}{M - j(1 + \gamma^{-\frac{1}{2}})^2} \right]^{\frac{1}{2}}. \tag{20}$$

   (c) Compute the test

$$T_j = \begin{cases} 1 & \text{if } \sigma_1(\mathbf{B}_j) > (1 + \gamma^{\frac{1}{2}} + r_\alpha)\hat{\sigma}_{{\rm n},j}, \\ 0 & \text{otherwise,} \end{cases} \tag{21}$$

   where the threshold value r_α is given by (15).
   (d) If $T_j = 1$ then define $\mathbf{B}_{j+1} = \mathbf{B}_j - \sigma_1(\mathbf{B}_j)\boldsymbol{u}_1(\mathbf{B}_j)\boldsymbol{v}_1(\mathbf{B}_j)^\dagger$, increase j by one, and go to (a). If $T_j = 0$ then set $\hat{r} = j - 1$ and $\hat{\sigma}_{\rm n} = \hat{\sigma}_{{\rm n},j-1}$ (if $j = 1$, then $\hat{\sigma}_{\rm n} = \hat{\sigma}_{{\rm n},0} = \|\mathbf{B}\|_F/(\gamma M)^{\frac{1}{2}}$) and go to 3.

The sequence of singular values $\sigma_1(\mathbf{B}_j)$, $j = 1, \dots, \hat{r}$, is the list of the $\hat{r}$ largest singular values $\sigma_j(\mathbf{B})$ of $\mathbf{B}$. Similarly the sequence of left singular vectors $\boldsymbol{u}_1(\mathbf{B}_j)$, $j = 1, \dots, \hat{r}$ is the list of the left singular vectors $\boldsymbol{u}_j(\mathbf{B})$ associated to the $\hat{r}$ largest singular values of $\mathbf{B}$. In fact, it is not necessary to compute explicitly the Frobenius norm of $\mathbf{B}_j$ at each step in 2(a). Indeed, we compute the Frobenius norm of $\mathbf{B}$ and then use the relation

$$\|\mathbf{B}_j\|_F^2 = \|\mathbf{B}\|_F^2 - \sum_{l=1}^{j-1} \sigma_1^2(\mathbf{B}_l),$$

or, equivalently, the recursive relation

$$\|\mathbf{B}_1\|_F^2 = \|\mathbf{B}\|_F^2, \qquad \|\mathbf{B}_{j+1}\|_F^2 = \|\mathbf{B}_j\|_F^2 - \sigma_1^2(\mathbf{B}_j), \quad j \geq 1.$$

This algorithm provides an estimator $\hat{\sigma}_{\rm n}$ of the noise level $\sigma_{\rm noise}$ and an estimator $\hat{r}$ of the number r of significant singular values, that is, the number of reflectors. The steps 3 and 4 of the previous algorithm are then used for the localization and characterization of the reflectors, using the estimator $\hat{\sigma}_{\rm n}$ for $\sigma_{\rm noise}$.

An alternative algorithm to estimate the noise level is based on the minimization of the Kolmogorov-Smirnov distance between the empirical distribution of the

(smallest) singular values of the perturbed matrix $\mathbf{B}$ and the theoretical deformed quarter-circle law [30]. This algorithm reduces significantly the bias but it is more computationally intensive. When M is very large, formula (20) is sufficient for the noise level estimation. When M is not very large, the algorithm presented in [30] should be used.

Instead of $\mathcal{I}_j(\boldsymbol{x})$ defined by (17), other subspace imaging functionals such as MUSIC or Kirchhoff-type algorithms can be used; see [11, 12, 17, 22, 41]. The decomposition of the time-reversal operator (DORT) can also be used [25, 26, 27, 29, 35] for detecting and characterizing the reflectors.

2.4. **Numerical simulations.** We consider the following numerical setup. The wavelength is equal to two (i.e., $\omega = \pi$, $c_0 = 1$). There are $r = 3$ reflectors with coefficients of reflection $\rho_1 = 2$, $\rho_2 = 1.5$, $\rho_3 = 1$, located at $\boldsymbol{x}_1 = (5, 0)$, $\boldsymbol{x}_2 = (-2.5, 4.33)$ and $\boldsymbol{x}_3 = (-2.5, -4.33)$. We consider a circular array of $M = 124$ transducers located (approximately) at half-a-wavelength apart on the circle of radius 20 centered at the origin. This array is used as a receiver and as a transmitter array (therefore, $N = M$ and $\gamma = 1$). The noise level varies from $\sigma_{\text{noise}} = \frac{2}{3}\sigma_3 (\simeq \frac{\sigma_1}{3})$ to $\sigma_{\text{noise}} = \sigma_3 (\simeq \frac{\sigma_1}{2})$, where σ_j is the singular value associated to the j-th reflector (given by (12)).

For each 20 levels of noise equi-distributed on the range of σ_{noise}, we have carried out a series of 10^3 Monte-Carlo (MC) simulations. It is worth emphasizing that the data are generated by a direct code without using the Born approximation. The results are the following ones:

- The first two reflectors are always detected. When the noise becomes too important the third one may be missed. Figure 1 shows the probability of detecting all three point reflectors as a function of the factor $\sigma_3/\sigma_{\text{noise}}$ given the false alarm rate $\alpha = 0.05$.

  We observe a sharp transition in the probability of detection of the third reflector. At given level of noise, the probability of detection depends on α. For example, when $\sigma_{\text{noise}} = \frac{4}{5}\sigma_1$, we find that for $\alpha = 0.1$, we have $\mathbb{P}(\hat{r} = 3) = 0.85$, for $\alpha = 0.05$, we have $\mathbb{P}(\hat{r} = 3) = 0.78$, and for $\alpha = 0.01$, we have $\mathbb{P}(\hat{r} = 3) = 0.63$.
- The estimators $\hat{\boldsymbol{x}}_j$ of the reflectors have good properties. The subspace imaging functional (17) gives excellent predictions as long as the first singular values and vectors correspond to the reflectors (and not to the noise).

  Figure 2 gives the mean and standard deviation for the estimation of the x and y coordinates of the three reflectors as a function of noise (for the third reflector, we use only the cases in which it has been detected). We can observe that the resolution is below the wavelength. This does not contradict classical diffraction limited results because we here use the a priori information that the reflectors are point-like.
- The estimators $\hat{\rho}_j$ of the reflectivities have small bias because they use the inversion formula (19) which compensates for the level of repulsion. We plot in Figure 3 the mean and standard deviation of the estimated reflectivities for the three reflectors as a function of noise (for the third reflector, we use only the cases in which it has been detected). We compare it to the empirical estimators:

$$\hat{\rho}_j^e = \Big(\sum_{n=1}^{N} |\hat{G}(\omega, \hat{\boldsymbol{x}}_j, \boldsymbol{y}_n)|^2 \Big)^{-\frac{1}{2}} \Big(\sum_{m=1}^{M} |\hat{G}(\omega, \hat{\boldsymbol{x}}_j, \boldsymbol{z}_m)|^2 \Big)^{-\frac{1}{2}} \sigma_j(\mathbf{B}), \tag{22}$$

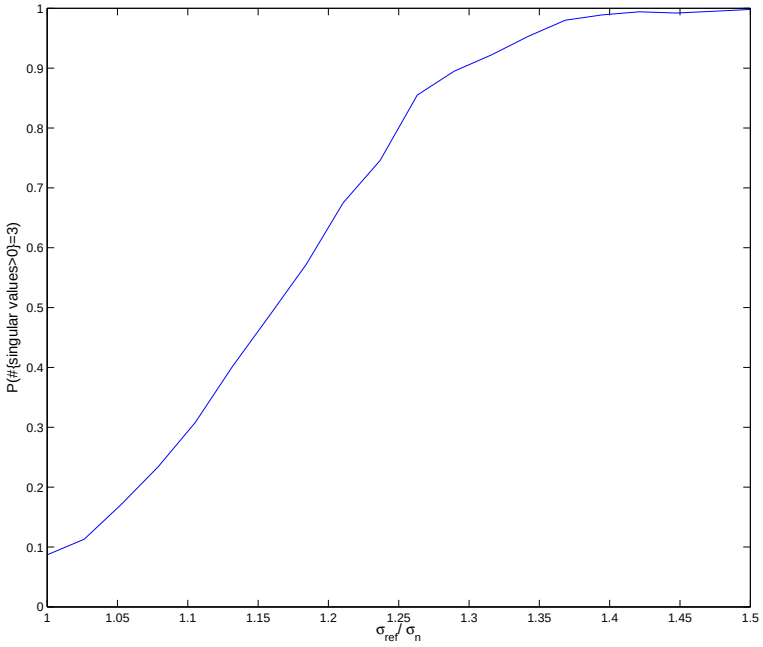

FIGURE 1. Probability of detecting all three point reflectors for $\alpha = 0.05$. Here $\sigma_{\rm ref} = \sigma_3(\mathbf{A})$.

which have obvious bias.

In the previous numerical simulations we have assumed that the noise level $\sigma_{\rm noise}$ was known. However in some practical applications the noise level has to be estimated. We have described an iterative algorithm to estimate the noise level. It has been implemented on the case of three point reflectors. Figure 4 gives the mean and standard deviation of the estimated noise level $\hat{\sigma}_{\rm noise}$ as a function of $\sigma_{\rm min}/\sigma_{\rm noise}$. As expected the estimator obtained with this algorithm has some bias. Nonetheless, our algorithm of detection and reconstruction of point reflectors still performs quite well with this noise estimation. If M were smaller then it would be necessary to use the Kolmogorov-Smirnov algorithm to estimate the noise level [30].

3. **Detection of small inclusions.**

3.1. **Asymptotic modelling of an inclusion.** In this section we consider the two-dimensional (electromagnetic) situation where an inclusion D with constant parameters $0 < \mu < +\infty$ and $0 < \varepsilon < +\infty$, $(\mu, \varepsilon) \neq (1, 1)$, is embedded into a background medium with permeability and permittivity equal to 1. Note that this situation is equivalent to an acoustic situation where an inclusion with anomalous density and compressibility is embedded into a homogeneous background medium. Suppose that $D = \tilde{D} + \boldsymbol{x}_{\rm inc}$, where $\tilde{D}$ is a small domain centered at $\mathbf{0}$, and $\boldsymbol{x}_{\rm inc}$ indicates the location of D. The time-harmonic field $\hat{u}(\boldsymbol{x}, \boldsymbol{y})$ observed at $\boldsymbol{x}$ when

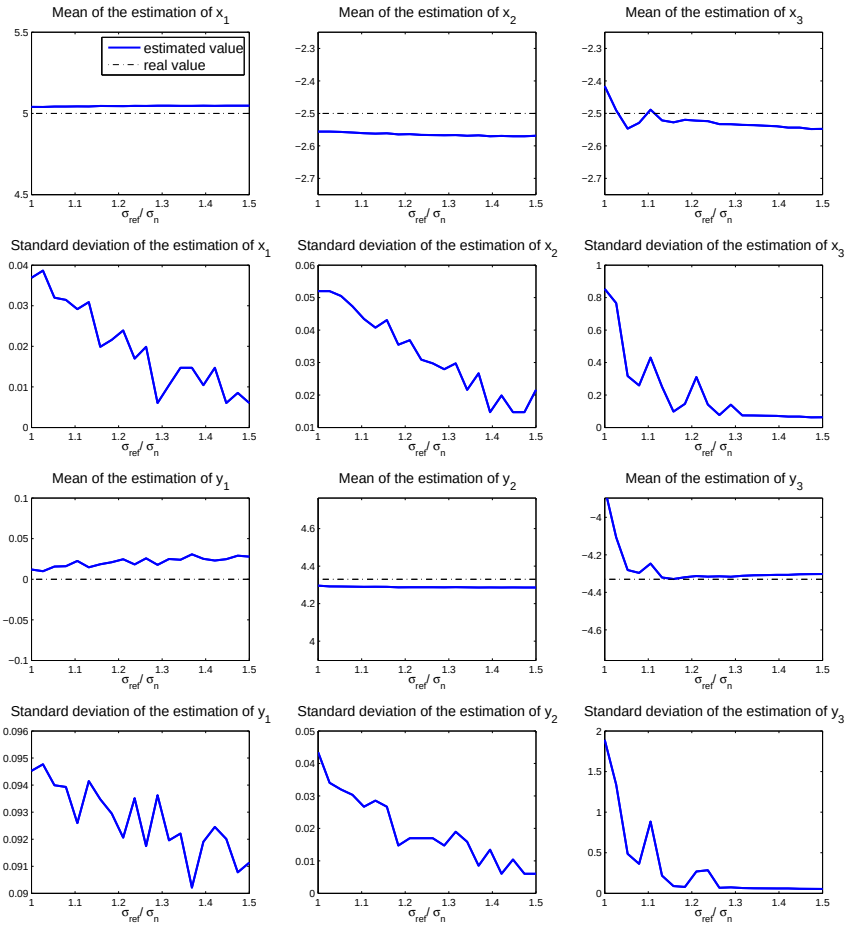

FIGURE 2. Mean and standard deviation for the estimation of the coordinates of the three point reflectors as a function of noise.

there is a point source at $\boldsymbol{z}$ is the solution of

$$\begin{cases} \nabla_{\boldsymbol{x}} \cdot \Big(1 + (\dfrac{1}{\mu} - 1)\mathbf{1}_D(\boldsymbol{x})\Big)\nabla_{\boldsymbol{x}}\hat{u} + \dfrac{\omega^2}{c_0^2}\big(1 + (\varepsilon - 1)\mathbf{1}_D(\boldsymbol{x})\big)\hat{u} = -\delta_{\boldsymbol{z}} \quad \text{in } \mathbb{R}^2, \\ \left|\Big(\dfrac{\partial}{\partial|\boldsymbol{x}|} - i\dfrac{\omega}{c_0}\Big)\Big(\hat{u}(\boldsymbol{x}) - \hat{G}(\omega, \boldsymbol{x}, \boldsymbol{z})\Big)\right| = \mathrm{O}(|\boldsymbol{x}|^{-3/2}), \end{cases} \tag{23}$$

where $\hat{G}$ is the time-harmonic Green's function given by (5).

Suppose that we have a transmitter array of M sources located at $\{\boldsymbol{z}_1, \ldots, \boldsymbol{z}_M\}$ and a receiver array of N elements located at $\{\boldsymbol{y}_1, \ldots, \boldsymbol{y}_N\}$. The $N \times M$ response matrix $\mathbf{A}$ is defined as in (4). The following asymptotic expression of the response

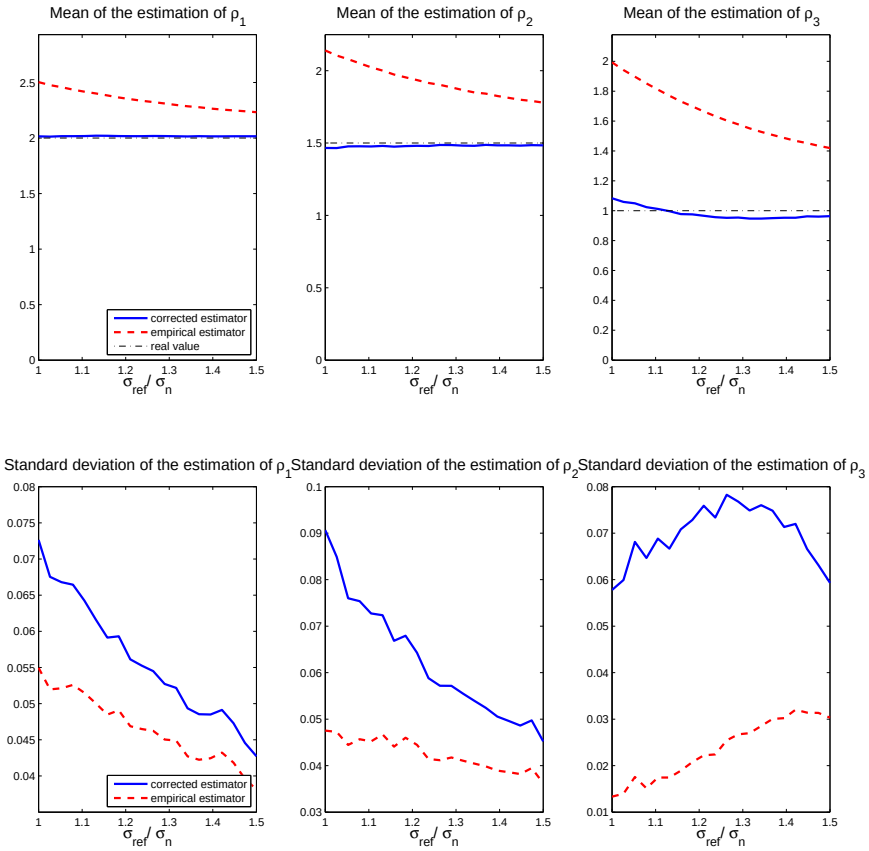

FIGURE 3. Mean and standard deviation of the estimated reflectivities for the three point reflectors as a function of noise.

matrix entries is established uniformly with respect to ω such that $\omega|\tilde{D}|^{1/2} < 1$

$$\begin{aligned} A_{nm} &= \nabla_{\boldsymbol{x}_{\rm inc}} \hat{G}(\omega, \boldsymbol{y}_n, \boldsymbol{x}_{\rm inc}) \cdot \mathbf{M}(\mu, \tilde{D}) \nabla_{\boldsymbol{x}_{\rm inc}} \hat{G}(\omega, \boldsymbol{x}_{\rm inc}, \boldsymbol{z}_m) \\ &\quad + \frac{\omega^2}{c_0^2}(\varepsilon - 1)|\tilde{D}| \hat{G}(\omega, \boldsymbol{y}_n, \boldsymbol{x}_{\rm inc}) \hat{G}(\omega, \boldsymbol{x}_{\rm inc}, \boldsymbol{z}_m) + o(\omega^2 |\tilde{D}|), \end{aligned} \tag{24}$$

when the volume $|\tilde{D}|$ of $\tilde{D}$ goes to zero. See [5, 14, 31, 40]. Here $\mathbf{M}(\mu, \tilde{D})$ is the polarization tensor given by [14, 15]:

$$\mathbf{M}(\mu, \tilde{D}) := (\frac{1}{\mu} - 1) \int_{\tilde{D}} \nabla(\hat{\boldsymbol{v}}(\tilde{\boldsymbol{x}}) + \tilde{\boldsymbol{x}}) d\tilde{\boldsymbol{x}},$$

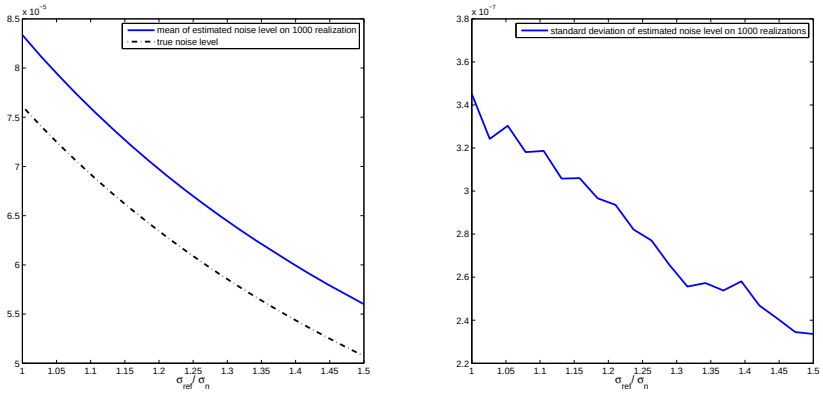

FIGURE 4. Mean and standard deviation of the estimated noise level $\hat{\sigma}_{\text{noise}}$ as a function of $\sigma_{\min}/\sigma_{\text{noise}}$.

where $\hat{\boldsymbol{v}}$ is the solution to

$$\begin{cases} \Delta\hat{\boldsymbol{v}} = \boldsymbol{0} \quad \text{in } \mathbb{R}^2 \setminus \overline{\tilde{D}}, \\ \Delta\hat{\boldsymbol{v}} = \boldsymbol{0} \quad \text{in } \tilde{D}, \\ \hat{\boldsymbol{v}}|_- - \hat{\boldsymbol{v}}|_+ = \boldsymbol{0} \quad \text{on } \partial\tilde{D}, \\ \dfrac{1}{\mu}\dfrac{\partial\hat{\boldsymbol{v}}}{\partial\nu}\Big|_- - \dfrac{\partial\hat{\boldsymbol{v}}}{\partial\nu}\Big|_+ = (\dfrac{1}{\mu} - 1)\boldsymbol{\nu} \quad \text{on } \partial\tilde{D}, \\ \hat{\boldsymbol{v}}(\tilde{\boldsymbol{x}}) \to 0 \quad \text{as } |\tilde{\boldsymbol{x}}| \to +\infty, \end{cases}$$

with $\boldsymbol{\nu}$ the outward-pointing unit normal vector.

A simplification (that is not necessary in the forthcoming analysis) consists in considering a high-frequency asymptotic expression for the Green's function. Using the asymptotic form of the Hankel function

$$H_0^{(1)}(x) \simeq \sqrt{2/(\pi|x|)}\exp(ix - i\,\mathrm{sgn}(x)\pi/4) \quad \text{for } |x| \gg 1,$$

we find that for $\omega|\boldsymbol{x}-\boldsymbol{y}|/c_0 \gg 1$ the Green's function takes the simple form:

$$\hat{G}(\omega,\boldsymbol{x},\boldsymbol{y}) \simeq \frac{\sqrt{c_0}}{2\sqrt{2\pi}}\frac{\exp(i\,\pi/4)}{\sqrt{\omega|\boldsymbol{y}-\boldsymbol{x}|}}\exp\Big(i\frac{\omega}{c_0}|\boldsymbol{y}-\boldsymbol{x}|\Big), \tag{25}$$

and

$$\nabla\hat{G}(\omega,\boldsymbol{x},\boldsymbol{y}) \simeq \frac{\sqrt{c_0}}{2\sqrt{2\pi}}\left(\frac{i\omega(\boldsymbol{x}-\boldsymbol{y})}{c_0|\boldsymbol{x}-\boldsymbol{y}|}\right)\frac{\exp(i\,\pi/4)}{\sqrt{\omega|\boldsymbol{x}-\boldsymbol{y}|}}\exp\Big(i\frac{\omega}{c_0}|\boldsymbol{x}-\boldsymbol{y}|\Big),$$

and hence the response matrix can be approximated by

$$\begin{aligned} A_{nm} \quad \simeq \quad & \frac{-i\omega}{8\pi c_0\sqrt{|\boldsymbol{y}_n-\boldsymbol{x}_{\text{inc}}||\boldsymbol{z}_m-\boldsymbol{x}_{\text{inc}}|}}\exp\Big(i\frac{\omega}{c_0}(|\boldsymbol{y}_n-\boldsymbol{x}_{\text{inc}}|+|\boldsymbol{z}_m-\boldsymbol{x}_{\text{inc}}|)\Big) \\ & \times\left[\frac{(\boldsymbol{y}_n-\boldsymbol{x}_{\text{inc}})\cdot\mathbf{M}(\mu,\tilde{D})(\boldsymbol{z}_m-\boldsymbol{x}_{\text{inc}})}{|\boldsymbol{y}_n-\boldsymbol{x}_{\text{inc}}||\boldsymbol{z}_m-\boldsymbol{x}_{\text{inc}}|} - |\tilde{D}|(\varepsilon-1)\right]. \end{aligned} \tag{26}$$

3.2. **The structure of the response matrix.** From now on we consider that there are R inclusions $(D_j)_{j=1,\dots,R}$ with parameters $0 < \mu_j < +\infty$ and $0 < \varepsilon_j < +\infty$ located in a background medium with permeability and permittivity equal to 1. Each inclusion is of the form $D_j = \tilde{D}_j + \boldsymbol{x}_j$. Further, we assume that the inclusions are small and far from each other (i.e., farther than the wavelength $2\pi c_0/\omega$). Then the response matrix can be approximately written in the form

$$\begin{aligned} A_{nm} \quad \simeq \quad & \sum_{j=1}^{R} \nabla_{\boldsymbol{x}} \hat{G}(\omega, \boldsymbol{x}_j, \boldsymbol{y}_n) \cdot \mathbf{M}(\mu_j, \tilde{D}_j) \nabla_{\boldsymbol{x}} \hat{G}(\omega, \boldsymbol{x}_j, \boldsymbol{z}_m) \\ & + \sum_{j=1}^{R} \frac{\omega^2}{c_0^2} (\varepsilon_j - 1) |\tilde{D}_j| \hat{G}(\omega, \boldsymbol{x}_j, \boldsymbol{y}_n) \hat{G}(\omega, \boldsymbol{x}_j, \boldsymbol{z}_m), \end{aligned}$$

where we have used the reciprocity relation $\hat{G}(\omega, \boldsymbol{x}, \boldsymbol{y}) = \hat{G}(\omega, \boldsymbol{y}, \boldsymbol{x})$. The tensor ($2 \times 2$ matrix) $\mathbf{M}(\mu_j, \tilde{D}_j)$ is diagonalizable:

$$\mathbf{M}(\mu_j, \tilde{D}_j) = \alpha_j \boldsymbol{a}(\theta_j) \boldsymbol{a}(\theta_j)^T + \beta_j \boldsymbol{a}(\theta_j + \pi/2) \boldsymbol{a}(\theta_j + \pi/2)^T,$$

where $\boldsymbol{a}(\theta) = (\cos\theta, \sin\theta)^T$. We can then write the matrix $\mathbf{A}$ in the form:

$$\mathbf{A} = \sum_{j=1}^{3R} \sigma_j \boldsymbol{u}_j \boldsymbol{v}_j^{\dagger}, \tag{27}$$

where

$$\begin{aligned} \sigma_{3(j-1)+1} \quad = \quad & \rho_j \Big(\sum_{n=1}^{N} |\hat{G}(\omega, \boldsymbol{x}_j, \boldsymbol{y}_n)|^2 \Big)^{\frac{1}{2}} \Big(\sum_{m=1}^{M} |\hat{G}(\omega, \boldsymbol{x}_j, \boldsymbol{z}_m)|^2 \Big)^{\frac{1}{2}}, \\ \sigma_{3(j-1)+2} \quad = \quad & \alpha_j \Big(\sum_{n=1}^{N} |\boldsymbol{a}(\theta_j)^T \nabla \hat{G}(\omega, \boldsymbol{x}_j, \boldsymbol{y}_n)|^2 \Big)^{\frac{1}{2}} \Big(\sum_{m=1}^{M} |\boldsymbol{a}(\theta_j)^T \nabla \hat{G}(\omega, \boldsymbol{x}_j, \boldsymbol{z}_m)|^2 \Big)^{\frac{1}{2}}, \\ \sigma_{3(j-1)+3} \quad = \quad & \beta_j \Big(\sum_{n=1}^{N} |\boldsymbol{a}(\theta_j + \pi/2)^T \nabla \hat{G}(\omega, \boldsymbol{x}_j, \boldsymbol{y}_n)|^2 \Big)^{\frac{1}{2}} \\ & \times \Big(\sum_{m=1}^{M} |\boldsymbol{a}(\theta_j + \pi/2)^T \nabla \hat{G}(\omega, \boldsymbol{x}_j, \boldsymbol{z}_m)|^2 \Big)^{\frac{1}{2}}, \end{aligned}$$

$\rho_j = \frac{\omega^2}{c_0^2}(\varepsilon_j - 1)|\tilde{D}_j|$, and

$$\begin{aligned} \boldsymbol{u}_{3(j-1)+1} \quad = \quad & \boldsymbol{u}(\boldsymbol{x}_j), \qquad \boldsymbol{v}_{3(j-1)+1} = \boldsymbol{v}(\boldsymbol{x}_j), \\ \boldsymbol{u}_{3(j-1)+2} \quad = \quad & \boldsymbol{U}(\boldsymbol{x}_j, \theta_j), \qquad \boldsymbol{v}_{3(j-1)+2} = \boldsymbol{V}(\boldsymbol{x}_j, \theta_j), \\ \boldsymbol{u}_{3(j-1)+3} \quad = \quad & \boldsymbol{U}(\boldsymbol{x}_j, \theta_j + \pi/2), \qquad \boldsymbol{v}_{3(j-1)+3} = \boldsymbol{V}(\boldsymbol{x}_j, \theta_j + \pi/2), \end{aligned}$$

with

$$\boldsymbol{U}(\boldsymbol{x}, \theta) \quad = \quad \frac{1}{\big(\sum_{l=1}^{N} |\boldsymbol{a}(\theta)^T \nabla \hat{G}(\omega, \boldsymbol{x}, \boldsymbol{y}_l)|^2 \big)^{\frac{1}{2}}} \big(\boldsymbol{a}(\theta)^T \nabla \hat{G}(\omega, \boldsymbol{x}, \boldsymbol{y}_n) \big)_{n=1,\dots,N}, \tag{28}$$

$$\boldsymbol{V}(\boldsymbol{x}, \theta) \quad = \quad \frac{1}{\big(\sum_{l=1}^{M} |\boldsymbol{a}(\theta)^T \nabla \hat{G}(\omega, \boldsymbol{x}, \boldsymbol{z}_l)|^2 \big)^{\frac{1}{2}}} \big(\overline{\boldsymbol{a}(\theta)^T \nabla \hat{G}(\omega, \boldsymbol{x}, \boldsymbol{z}_m)} \big)_{m=1,\dots,M}. \tag{29}$$

Note that (27) is not a priori a singular value decomposition, since the vectors $\boldsymbol{u}_j$ (and $\boldsymbol{v}_j$) may not be orthogonal. However, as in the previous section, the orthogonality condition is guaranteed provided that:

- the positions $\boldsymbol{x}_j$ of the inclusions are far from each other (i.e., much farther than the wavelength),
- the sensors cover the surface of a disk or a sphere surrounding the search region.

The second condition ensures the orthogonality of the three vectors associated to the same inclusion (using the Helmholtz-Kirchhoff identity). The first condition ensures the orthogonality of the vectors associated to different inclusions. When these two conditions are fulfilled, the vectors $\boldsymbol{u}_j$, $j = 1, \ldots, 3R$, are approximately orthogonal to each other, as well as the vectors $\boldsymbol{v}_j$, $j = 1, \ldots, 3R$. The matrix $\mathbf{A}$ has then rank $3R$ and its non-zero singular values are σ_j, $j = 1, \ldots, 3R$, with the associated left and right singular vectors $\boldsymbol{u}_j$ and $\boldsymbol{v}_j$.

3.3. **Singular vectors of the perturbed response matrix.** Taking into account measurement noise, the measured response matrix $\mathbf{B}$ is

$$\mathbf{B} = \mathbf{A} + \frac{1}{\sqrt{M}}\mathbf{W}, \tag{30}$$

where the matrix $\mathbf{A}$ is the unperturbed matrix (27) and the matrix $\mathbf{W}$ represents the additive measurement noise, which is a random matrix with independent and identically distributed complex entries with Gaussian statistics, mean zero and variance σ^2_{noise}. The singular values of the perturbed matrix $\mathbf{B}$ and of the unperturbed matrix $\mathbf{A}$ are related as described in Theorem 2.1. It is of interest to describe the statistical distribution of the angles between the left and right singular vectors $\boldsymbol{u}_j(\mathbf{B})$ and $\boldsymbol{v}_j(\mathbf{B})$ of the noisy matrix $\mathbf{B}$ with respect to the left and right singular vectors $\boldsymbol{u}_j(\mathbf{A})$ and $\boldsymbol{v}_j(\mathbf{A})$ of the unperturbed matrix $\mathbf{A}$. This plays a key role in the algorithm that we discuss in Section 3.4.

Theorem 3.1. *We assume the same conditions as in Theorem 2.1 and moreover that the non-zero singular values $\sigma_j^2(\mathbf{A})$ are distinct. When $\gamma = N/M$ and R are fixed and $M \to \infty$, for any $j = 1, \ldots, 3R$ such that $\sigma_j(\mathbf{A}) > \gamma^{\frac{1}{4}}\sigma_{\text{noise}}$, we have*

$$\left|\boldsymbol{u}_j(\mathbf{A})^\dagger \boldsymbol{u}_j(\mathbf{B})\right|^2 \overset{M\to\infty}{\longrightarrow} \frac{1 - \gamma \frac{\sigma^4_{\text{noise}}}{\sigma_j^4(\mathbf{A})}}{1 + \gamma \frac{\sigma^2_{\text{noise}}}{\sigma_j^2(\mathbf{A})}} \tag{31}$$

and

$$\left|\boldsymbol{v}_j(\mathbf{A})^\dagger \boldsymbol{v}_j(\mathbf{B})\right|^2 \overset{M\to\infty}{\longrightarrow} \frac{1 - \gamma \frac{\sigma^4_{\text{noise}}}{\sigma_j^4(\mathbf{A})}}{1 + \frac{\sigma^2_{\text{noise}}}{\sigma_j^2(\mathbf{A})}} \tag{32}$$

in probability.

Theorem 3.1 is proved in Appendix B. It shows that the cosines of the angles between the singular vectors of the perturbed matrix $\mathbf{B}$ and the singular vectors of the unperturbed matrix $\mathbf{A}$ are deterministic provided the corresponding perturbed singular values emerge from the deformed quarter-circle distribution. Although we will not give the proof of the following result (which we will not use in the sequel), we also have, for any $j = 1, \ldots, 3R$ such that $\sigma_j(\mathbf{A}) \le \gamma^{\frac{1}{4}}\sigma_{\text{noise}}$,

$$\left|\boldsymbol{u}_j(\mathbf{A})^\dagger \boldsymbol{u}_j(\mathbf{B})\right|^2 \overset{M\to\infty}{\longrightarrow} 0 \quad \text{and} \quad \left|\boldsymbol{v}_j(\mathbf{A})^\dagger \boldsymbol{v}_j(\mathbf{B})\right|^2 \overset{M\to\infty}{\longrightarrow} 0 \tag{33}$$

in probability.

3.4. **Algorithm for detection, localization, and reconstruction.** We first apply Steps 1 and 2 of the algorithm described in Section 2.3 to estimate the number $\hat{r}$ of significant singular values of the perturbed matrix $\mathbf{B}$. We apply either the first version, in the case in which the noise level is known, or the second one, in the case in which it is unknown. We use in the following the same notation as in Section 2.3. The sequence of singular values $\sigma_1(\mathbf{B}_j)$, $j = 1, \dots, \hat{r}$ is the list of the $\hat{r}$ largest singular values $\sigma_j(\mathbf{B})$ of $\mathbf{B}$. Similarly the sequence of left singular vectors $\boldsymbol{u}_1(\mathbf{B}_j)$, $j = 1, \dots, \hat{r}$, is the list of the left singular vectors $\boldsymbol{u}_j(\mathbf{B})$ associated to the $\hat{r}$ largest singular values of $\mathbf{B}$.

The following steps are original compared to the previous algorithm. Indeed, in Section 2.3, the singular vectors are all of the same form. Here the singular vectors may have different forms depending on their nature (dielectric or magnetic).

3. For each $j = 1, \dots, \hat{r}$, we consider the two functionals

$$\mathcal{I}_j(\boldsymbol{x}) = |\boldsymbol{u}(\boldsymbol{x})^\dagger \boldsymbol{u}_j(\mathbf{B})|^2, \qquad \mathcal{J}_j(\boldsymbol{x}, \theta) = |\mathbf{U}(\boldsymbol{x}, \theta)^\dagger \boldsymbol{u}_j(\mathbf{B})|^2,$$

where $\mathbf{U}(\boldsymbol{x}, \theta)$ is given by (28). We find their maxima $\mathcal{I}_{j,max}$ and $\mathcal{J}_{j,max}$ (the optimization with respect to θ for $\mathcal{J}_j(\boldsymbol{x}, \theta)$ can be carried out analytically). We estimate the theoretical angle between the unperturbed and perturbed vectors by

$$\hat{c}_j = \frac{1 - \gamma \frac{\sigma_{\rm noise}^4}{\hat{\sigma}_j^4}}{1 + \gamma \frac{\sigma_{\rm noise}^2}{\hat{\sigma}_j^2}},$$

with $\hat{\sigma}_j$ the estimator of $\sigma_j(\mathbf{A})$ given by (19). We decide of the type (`d` for dielectric, `m` for magnetic) of the jth singular value as follows:

$$\mathcal{T}_j = \begin{cases} \texttt{d} & \text{if } |\mathcal{I}_{j,max} - \hat{c}_j| \le |\mathcal{J}_{j,max} - \hat{c}_j|, \\ \texttt{m} & \text{if } |\mathcal{I}_{j,max} - \hat{c}_j| > |\mathcal{J}_{j,max} - \hat{c}_j|. \end{cases}$$

We also record the position $\hat{\boldsymbol{x}}_j$ of the maximum of the imaging functional $\mathcal{I}_j(\boldsymbol{x})$ if $\mathcal{T}_j = \texttt{d}$ or the position and angle $(\hat{\boldsymbol{x}}_j, \hat{\theta}_j)$ of the maximum of the imaging functional $\mathcal{J}_j(\boldsymbol{x}, \theta)$ if $\mathcal{T}_j = \texttt{m}$.

4. We now cluster the results: we consider the set of positions $\hat{x}_j$ estimated in Step 3. We group the indices $\{1, \dots, \hat{r}\}$ in subsets $(I_q)_{q=1,\dots,\hat{R}}$ of up to three indices which contain the indices that correspond to positions close to each other (within one wavelength):

   Set $I = \{2, \dots, \hat{r}\}$, $j = 1$, $q = 1$, and $I_1 = \{1\}$.
   While $I \neq \emptyset$, do
   - consider $\tilde{I} = \{l \in I \text{ such that } |\hat{\boldsymbol{x}}_l - \hat{\boldsymbol{x}}_j| < \lambda, \mathcal{T}_l \text{ is compatible}\}$.
   - if $\tilde{I} = \emptyset$, then increase q by one, set $j = \min(I)$, $I_q = \{j\}$, and remove j from I.
   - if $\tilde{I} \neq \emptyset$, then add $\min(\tilde{I})$ into I_q and remove it from I.

   We say that the type $\mathcal{T}_l$ is not compatible if it is `d` in the case in which there is already one index with type `d` in I_q, or if it is `m` in the case in which there are already two indices with type `m` in I_q (note that this implies that $\mathcal{T}_l$ is never compatible as soon as $|I_q| = 3$)

   This procedure gives the decomposition:

$$\{1, \dots, \hat{r}\} = \cup_{q=1}^{\hat{R}} I_q, \qquad I_q = \{j_1^{(q)}, \dots, j_{n_q}^{(q)}\},$$

with $1 \leq n_q \leq 3$. The subset I_q contains n_q indices that correspond to positions close to each other and it does not contain two indices with type $\mathtt{d}$ or three indices with type $\mathtt{m}$.

The estimators of the relevant quantities are the following ones:
The number of inclusions is estimated by $\hat{R}$.
The position of the q-th inclusion is estimated by the barycenter (Method 1):

$$\hat{\boldsymbol{X}}_q = \frac{1}{n_q} \sum_{l=1}^{n_q} \hat{\boldsymbol{x}}_{j_l^{(q)}}$$

An alternative estimator (Method 2) is obtained by an optimization method. It is given by

$$\hat{\boldsymbol{X}}_q = \operatorname*{argmax}_{\boldsymbol{x}} \Big\{ \sum_{l=1}^{n_q} \sigma_{j_l^{(q)}}(\mathbf{B})^2 \Big[\mathbf{1}_{\mathcal{T}_{j_l^{(q)}}=\mathtt{d}} \big| \boldsymbol{u}(\boldsymbol{x})^\dagger \boldsymbol{u}_{j_l^{(q)}}(\mathbf{B}) \big|^2 + \mathbf{1}_{\mathcal{T}_{j_l^{(q)}}=\mathtt{m}} \big| \mathbf{U}(\boldsymbol{x}, \hat{\theta}_{j_l^{(q)}})^\dagger \boldsymbol{u}_{j_l^{(q)}}(\mathbf{B}) \big|^2 \Big] \Big\}.$$

The first estimator can be used as a first guess for Method 2. More exactly the second estimator can be implemented in the form of an iterative algorithm (steepest descent) starting from this first guess.

The dielectric coefficients ρ_q of the q-th inclusion cannot be estimated if there is no index with type $\mathtt{d}$ in I_q, otherwise it can be estimated by

$$\hat{\rho}_q = \Big(\sum_{n=1}^{N} |\hat{G}(\omega, \hat{\boldsymbol{X}}_q, \boldsymbol{y}_n)|^2 \Big)^{-\frac{1}{2}} \Big(\sum_{m=1}^{M} |\hat{G}(\omega, \hat{\boldsymbol{X}}_q, \boldsymbol{z}_m)|^2 \Big)^{-\frac{1}{2}} \hat{\sigma}_{j_l^{(q)}}, \tag{34}$$

with $\hat{\sigma}_j$ the estimator of $\sigma_j(\mathbf{A})$ given by (19) and $j_l^{(q)}$ is here the index with type $\mathtt{d}$ in I_q.

The angle and the magnetic coefficient α and β of the q-th inclusion:
- cannot be estimated if there is no index with type $\mathtt{m}$ in I_q,
- can be estimated by

$$\hat{\Theta}_q = \hat{\theta}_{j_l^{(q)}},$$
$$\hat{\alpha}_q = \Big(\sum_{n=1}^{N} |\boldsymbol{a}(\hat{\Theta}_q)^T \nabla \hat{G}(\omega, \hat{\boldsymbol{X}}_q, \boldsymbol{y}_n)|^2 \Big)^{-\frac{1}{2}} \Big(\sum_{m=1}^{M} |\boldsymbol{a}(\hat{\Theta}_q)^T \nabla \hat{G}(\omega, \hat{\boldsymbol{X}}_q, \boldsymbol{z}_m)|^2 \Big)^{-\frac{1}{2}} \hat{\sigma}_{j_l^{(q)}},$$

if there is one index $j_l^{(q)}$ with type $\mathtt{m}$ in I_q,
- can be estimated by

$$\begin{aligned} \hat{\Theta}_q &= \operatorname*{argmax}_{\theta} \big\{ \sigma_{j_l^{(q)}}(\mathbf{B})^2 |\mathbf{U}(\hat{\boldsymbol{X}}_q, \theta)^\dagger \boldsymbol{u}_{j_l^{(q)}}(\mathbf{B})|^2 \\ &\qquad + \sigma_{j_{l'}^{(q)}}(\mathbf{B})^2 |\mathbf{U}(\hat{\boldsymbol{X}}_q, \pi/2 + \theta)^\dagger \boldsymbol{u}_{j_{l'}(q)}(\mathbf{B})|^2 \big\}, \\ \hat{\alpha}_q &= \Big(\sum_{n=1}^{N} |\boldsymbol{a}(\hat{\Theta}_q)^T \nabla \hat{G}(\omega, \hat{\boldsymbol{X}}_q, \boldsymbol{y}_n)|^2 \Big)^{-\frac{1}{2}} \\ &\quad \times \Big(\sum_{m=1}^{M} |\boldsymbol{a}(\hat{\Theta}_q)^T \nabla \hat{G}(\omega, \hat{\boldsymbol{X}}_q, \boldsymbol{z}_m)|^2 \Big)^{-\frac{1}{2}} \hat{\sigma}_{j_l^{(q)}}, \end{aligned}$$

$$\hat{\beta}_q = \Big(\sum_{n=1}^{N} |\boldsymbol{a}(\hat{\Theta}_q + \pi/2)^T \nabla \hat{G}(\omega, \hat{\boldsymbol{X}}_q, \boldsymbol{y}_n)|^2\Big)^{-\frac{1}{2}} \times \Big(\sum_{m=1}^{M} |\boldsymbol{a}(\hat{\Theta}_q + \pi/2)^T \nabla \hat{G}(\omega, \hat{\boldsymbol{X}}_q, \boldsymbol{z}_m)|^2\Big)^{-\frac{1}{2}} \hat{\sigma}_{j_{l'}^{(q)}},$$

if there are two indices $j_l^{(q)}, j_{l'}^{(q)}$ with type $\mathtt{m}$ in I_q.

3.5. **Numerical simulations.** We illustrate the algorithm proposed for small-volume inclusions in the following numerical setting. The operating wavelength is equal to 2 ($\omega = \pi$, $c_0 = 1$). As shown in Figure 5, there are 3 inclusions located at $\boldsymbol{x}_1 = (5, 0)$, $\boldsymbol{x}_2 = (-2.5, 4.33)$ and $\boldsymbol{x}_3 = (-2.5, -4.33)$, with parameters $(\epsilon_1, \mu_1) = (2, 2)$, $(\epsilon_2, \mu_2) = (1, 3)$ and $(\epsilon_3, \mu_3) = (3, 1)$. The inclusions are disks of the same radius $\delta = 0.01$.

We consider an array of $N = M = 124$ receivers-transmitters equi-distributed along the circle centered at the origin and of radius 20. As said before, we have to consider full aperture data otherwise the orthogonality between the vectors $\boldsymbol{u}$ and $\mathbf{U}$ corresponding to a given inclusion is not guaranteed. Again, it is worth emphasizing that the data is generated by a direct code without using the small-volume approximation (24).

We consider 20 (known) noise levels ranging from 2/3 to 1 times the smallest singular value $\sigma_{\text{ref}} = \sigma_6(\mathbf{A})$. Each time, we carry out 10^3 MC simulations. We set the false alarm rate $\alpha = 0.05$.

3.5.1. *Estimation of the number of singular values and classification of the singular vectors.* In Figure 6 an example of the discrepancy of the singular values is given for one realization when $\sigma_{\text{noise}} = 0.95\ \sigma_{\text{ref}}$. The theoretical response matrix $\mathbf{A}$ has 6 significant singular values. From largest to smallest, we have one for the dielectric effect of the third inclusion ($\epsilon_3 = 3$), one for the dielectric effect of the first inclusion ($\epsilon_1 = 2$), two for the magnetic effect of the second inclusion ($\mu_2 = 3$) and two for the magnetic effect of the first inclusion ($\mu_1 = 2$). In this realization, the detection of the sixth singular value has failed.

Figure 7 gives the estimated probability of detecting all the 6 singular values as a function of the noise level. We also plot in Figure 8 the classification achieved by the algorithm. The exact classification (detection of the 6 singular values and correct attribution of their physical source= dark red) is achieved for the weakest level of noise (right side of the graph). For stronger noise, the orange and blue parts correspond to missing singular values but good classification of the detected ones. On the contrary, the red and light blue parts correspond to misclassification of singular values and may reveal more troublesome. For example when $\sigma_{\text{ref}}/\sigma_{\text{noise}} \simeq 1.35$, the sixth singular value is detected most of the time but is misclassified more than half the time. This results in the appearing of an artifact dielectric inclusion at the same location as the true electromagnetic inclusion 1.

3.5.2. *Estimation of the position and the parameters of the inclusions.* Figures 9, 10, and 11 give the mean and standard deviation of the positions and electromagnetic parameters of the inclusions identified through the algorithm.

We observe that the estimation of the position of the inclusions is almost unaffected by the noise level. This is because each inclusion has singular values well above the noise level. Even if the magnetic part (singular values 5 and 6) of the inclusion 1 is missed or misinterpreted, its dielectric part is always identified (singular

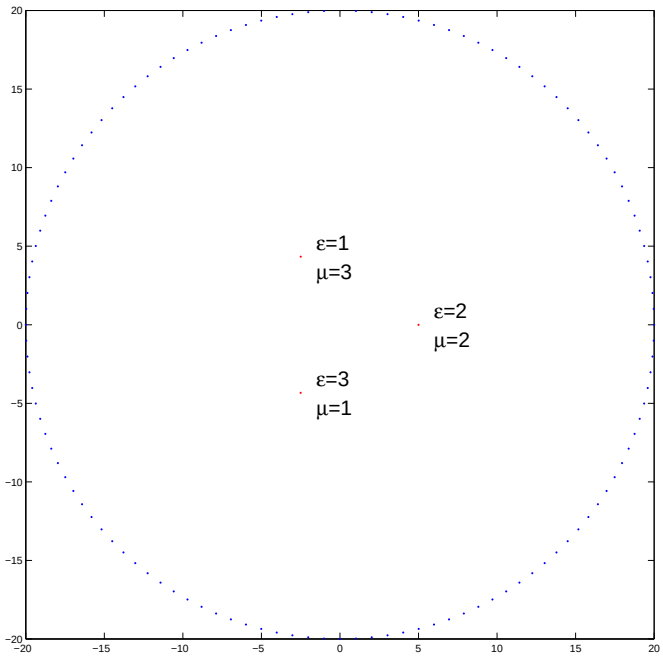

FIGURE 5. Configuration: three small-volume disk-shaped inclusions with different electromagnetic parameters. The separation distance between the inclusions is larger than the wavelength.

value 2). Estimation of the position (x_3, y_3) of the third inclusion (corresponding to the largest singular values) has no variability and its bias is smaller than the pixel size on the search domain.

Once again, the estimation of the parameters of the inclusions seems unaffected on this range of noise. Since singular values 5 and 6 are not always detected, α_1 cannot always be estimated. The mean and standard deviation are then estimated only on the subset of realization where at least one of the corresponding singular values is detected.

4. **Conclusion.** In this work, original algorithms for detecting, locating, and characterizing point reflectors and small inclusions from noisy response matrices have been introduced. Our algorithms are based on analytical formulas for the statistical distributions of the eigenvalues (in the case of point reflectors) and the angles between the left and right singular vectors (in the case of small inclusions). We have successfully tested the proposed algorithms and numerically shown their efficiency. It would be very interesting to generalize the present approach to the limited-view case. Since the orthogonality property satisfied by the normalized vectors of Green's function from the receiver or transmitter array to the center of the inclusions is no more valid in the limited-view case, the analysis would be quite involved. We will also make an attempt to extend the approach introduced in this paper to full

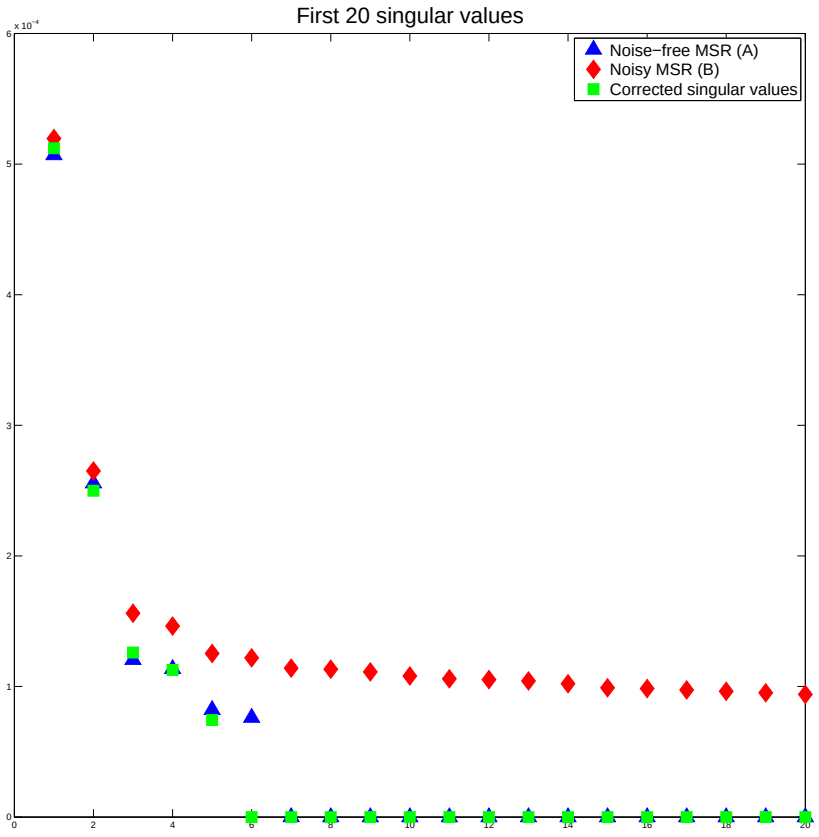

FIGURE 6. Discrepancy of the singular values for one realization with $\sigma_{\text{noise}} = 0.95\ \sigma_{\text{ref}}$.

Maxwell's equations and to linear elasticity, as well. Imaging electromagnetic and elastic small inclusions from response matrices was originally developed in [13, 3].

Appendix A. **Proof of Theorem 2.1.** If $\mathbf{X}$ is an $N \times M$ matrix, then we denote by $\sigma_j(\mathbf{X})$, $j = 1, \ldots, N \wedge M$, the singular values of $\mathbf{X}$. If $\mathbf{X}$ is a diagonalizable $M \times M$ matrix, then we denote by $\lambda_j(\mathbf{X})$, $j = 1, \ldots, M$, the eigenvalues of $\mathbf{X}$.

Step 1. We briefly summarize some known results about the spiked population model. The spiked population model is a random matrix model for $N \times M$ matrices introduced in [33].

Let r be a positive integer. Let $l_1 \geq \cdots \geq l_r > 1$ be positive real numbers. We define the $N \times N$ population covariance matrix by $\mathbf{\Sigma} = \text{diag}(l_1, \ldots, l_r, 1, \ldots, 1)$. We consider the random matrix $\mathbf{X}$ whose M columns are independent realizations of complex Gaussian vectors with mean zero and covariance $\mathbf{\Sigma}$. We introduce the

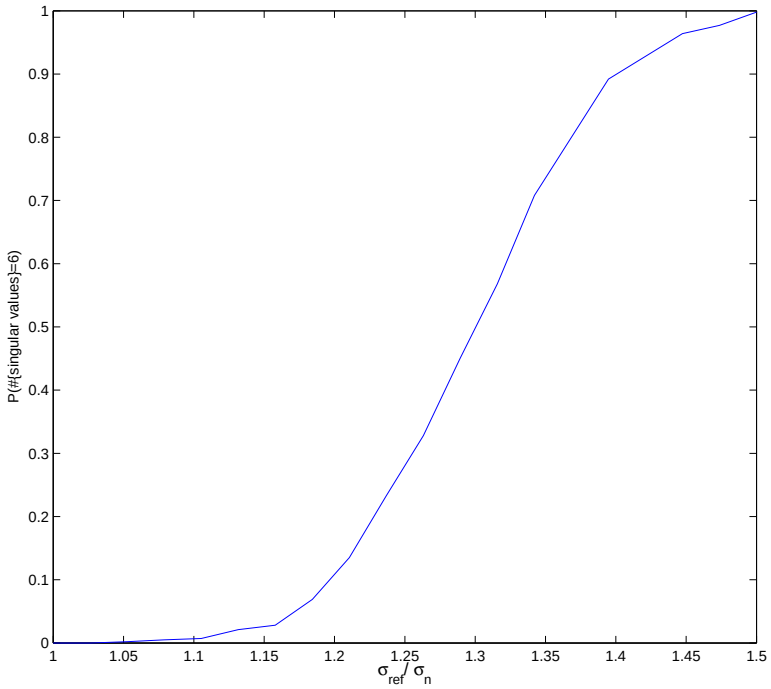

FIGURE 7. Estimated probability of detecting all the 6 singular values as a function of the noise level.

sample covariance matrix

$$\mathbf{S_X} = \frac{1}{M}\mathbf{X}\mathbf{X}^\dagger.$$

The statistical behavior of the eigenvalues $\lambda_j(\mathbf{S_X})$, $j = 1, \ldots, N$ has been obtained in [21] when $\gamma = N/M$ is fixed and $N \to \infty$:

Lemma A.1. *When $\gamma = N/M$ is fixed and $M \to \infty$ we have for $j = 1, \ldots, r$:*

$$\lambda_j(\mathbf{S_X}) \overset{M\to\infty}{\longrightarrow} \begin{cases} l_j + \gamma \dfrac{l_j}{l_j - 1} & \text{if } l_j > 1 + \gamma^{\frac{1}{2}}, \\ \left(1 + \gamma^{\frac{1}{2}}\right)^2 & \text{if } l_j \leq 1 + \gamma^{\frac{1}{2}}, \end{cases}$$

almost surely.

We write the random matrix $\mathbf{X}$ as

$$\mathbf{X} = \mathbf{Y} + \mathbf{Z},$$

where $\mathbf{Y}$ and $\mathbf{Z}$ are independent, the M columns of $\mathbf{Y}$ are independent realizations of complex Gaussian vectors with mean zero and covariance $\mathbf{\Sigma} - \mathbf{I}$ and the M columns of $\mathbf{Z}$ are independent realizations of complex Gaussian vectors with mean zero and covariance $\mathbf{I}$. In other words $\mathbf{Z}$ have independent and identically complex entries with mean zero and variance one. Note also that the entries Y_{nm} of $\mathbf{Y}$ are zero if $n \geq r + 1$ (almost surely), since they are realizations of Gaussian random

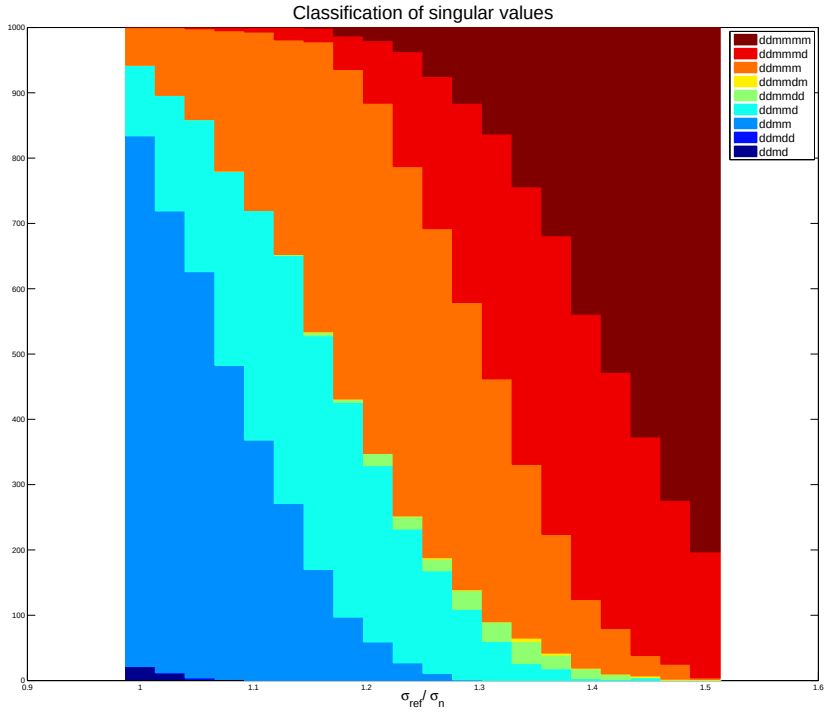

FIGURE 8. Classification of the inclusions as a function of the noise level. Dark red corresponds to detection of the 6 singular values and correct attribution of their physical source. Orange and blue parts correspond to missing singular values but good classification of the detected ones. Red and light blue parts correspond to misclassification of singular values.

variables with mean zero and variance zero. Therefore:
- the matrix $\mathbf{Y}$ has the form

$$\mathbf{Y} = \begin{pmatrix} \widetilde{\mathbf{Y}} \\ \mathbf{0} \end{pmatrix},$$

where $\widetilde{\mathbf{Y}}$ is a $r \times M$ random matrix whose M columns are independent realizations of complex Gaussian vectors with mean 0 and $r \times r$ covariance matrix $\widetilde{\mathbf{\Sigma}} = \mathrm{diag}(l_1 - 1, \ldots, l_r - 1)$.
- the sample covariance matrix $\mathbf{S_Y} = \frac{1}{M}\mathbf{Y}\mathbf{Y}^\dagger$ has the form

$$\mathbf{S_Y} = \begin{pmatrix} \widetilde{\mathbf{S}}_{\widetilde{\mathbf{Y}}} & \mathbf{0} \\ \mathbf{0} & \mathbf{0} \end{pmatrix},$$

where $\widetilde{\mathbf{S}}_{\widetilde{\mathbf{Y}}} = \frac{1}{M}\widetilde{\mathbf{Y}}\widetilde{\mathbf{Y}}^\dagger$. $\widetilde{\mathbf{S}}_{\widetilde{\mathbf{Y}}}$ is a $r \times r$ matrix with entries $(\widetilde{\mathbf{S}}_{\widetilde{\mathbf{Y}}})_{qq'} = \frac{1}{M}\sum_{m=1}^{M} \widetilde{Y}_{qm}\overline{\widetilde{Y}_{q'm}}$. By the law of large numbers we have

$$\widetilde{\mathbf{S}}_{\widetilde{\mathbf{Y}}} \overset{M\to\infty}{\longrightarrow} \widetilde{\mathbf{\Sigma}},$$

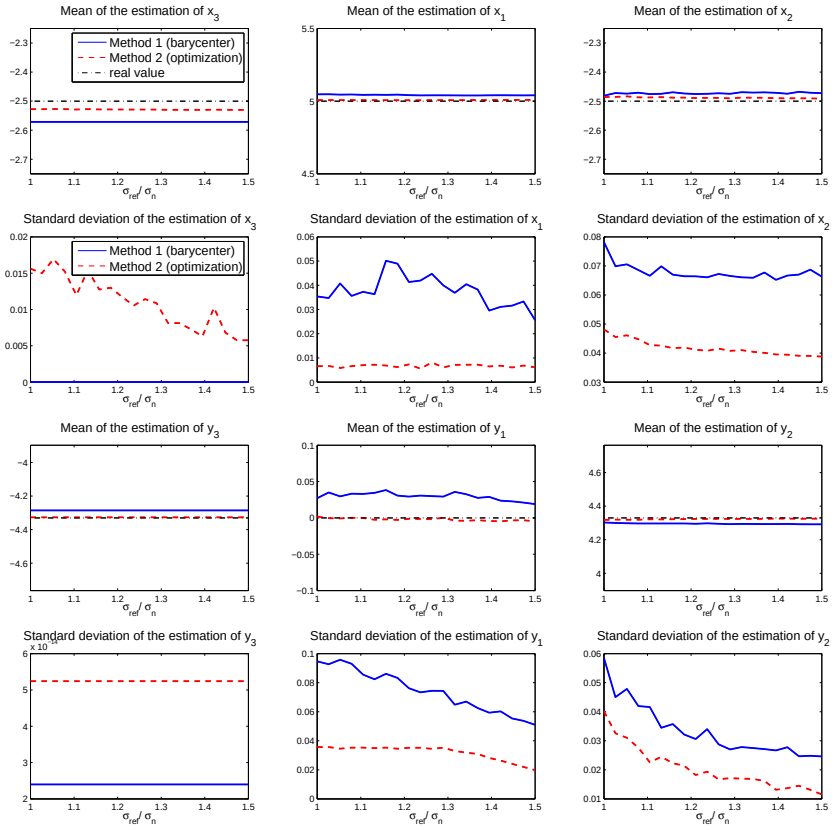

FIGURE 9. Mean and standard deviation of the positions of the inclusions.

almost surely. The almost sure convergence to zero of the Frobenius norm $\|\widetilde{\mathbf{S}}_{\widetilde{\mathbf{Y}}} - \widetilde{\mathbf{\Sigma}}\|_F$ also holds. Since we have for $j = 1, \ldots, r$

$$\sigma_j\big(\frac{1}{\sqrt{M}}\mathbf{Y}\big)^2 = \lambda_j\big(\frac{1}{M}\mathbf{Y}\mathbf{Y}^\dagger\big) = \lambda_j(\mathbf{S}_\mathbf{Y}) = \lambda_j(\widetilde{\mathbf{S}}_{\widetilde{\mathbf{Y}}}),$$

we find that

$$\sigma_j\big(\frac{1}{\sqrt{M}}\mathbf{Y}\big) \overset{M\to\infty}{\longrightarrow} \lambda_j(\widetilde{\mathbf{\Sigma}})^{\frac{1}{2}} = \sqrt{l_j - 1}, \tag{35}$$

almost surely. Note also that, for $j \geq r+1$ we have $\sigma_j\big(\frac{1}{\sqrt{M}}\mathbf{Y}\big) = 0$.

Step 2. Let $\mathbf{A}$ be an $N \times M$ rank-r deterministic matrix whose nonzero singular values are $\sigma_1(\mathbf{A}) \geq \cdots \geq \sigma_r(\mathbf{A}) > 0$. Let $\mathbf{W}$ be an $N \times M$ random matrix with independent and identically distributed complex entries with Gaussian statistics, mean zero and variance one (i.e., the real and imaginary parts of the entries are independent and obey real Gaussian distribution with mean zero and variance $1/2$).

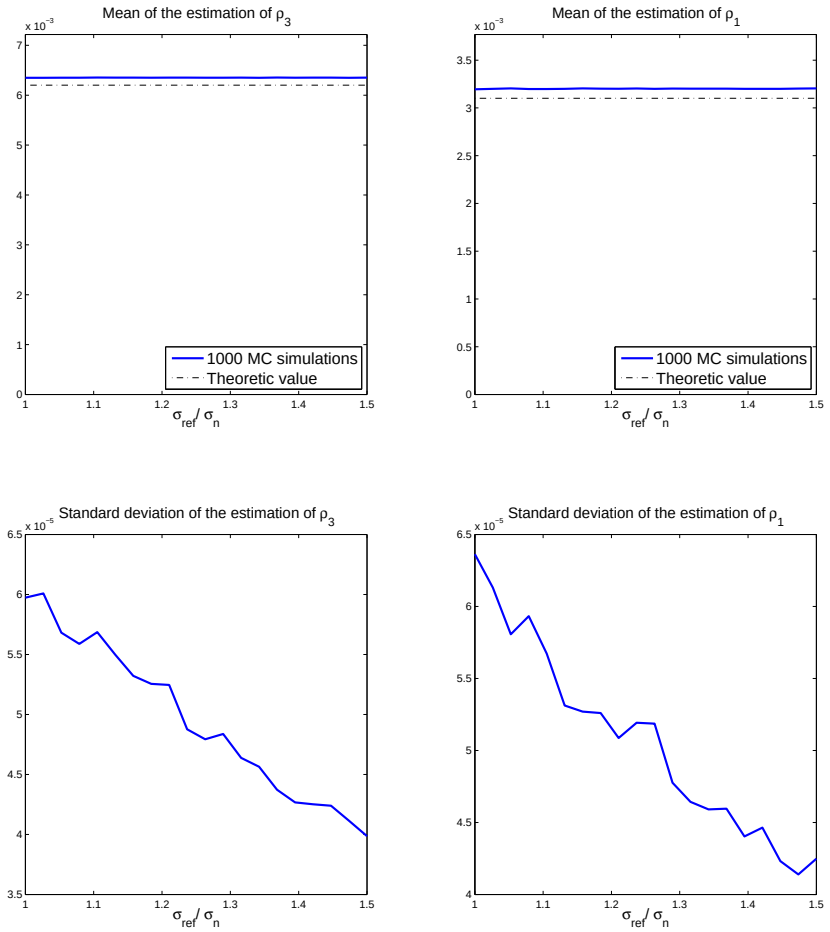

FIGURE 10. Mean and standard deviation of the parameter ρ of the inclusions.

We define

$$\mathbf{B} = \mathbf{A} + \frac{1}{\sqrt{M}}\mathbf{W}. \tag{36}$$

Lemma A.2. *When $\gamma = N/M$ is fixed and $M \to \infty$, for any $j = 1, \dots, r$,*

$$\sigma_j(\mathbf{B}) \overset{M\to\infty}{\longrightarrow} \begin{cases} \left(l_j + \gamma \dfrac{l_j}{l_j - 1}\right)^{\frac{1}{2}} & \text{if } l_j > 1 + \gamma^{\frac{1}{2}}, \\ 1 + \gamma^{\frac{1}{2}} & \text{if } l_j \leq 1 + \gamma^{\frac{1}{2}}, \end{cases}$$

in probability, with $l_j = 1 + \sigma_j(\mathbf{A})^2$.

Proof. We first establish a relationship between the perturbed model (36) and a spiked population model. The idea to use such a relationship was proposed recently

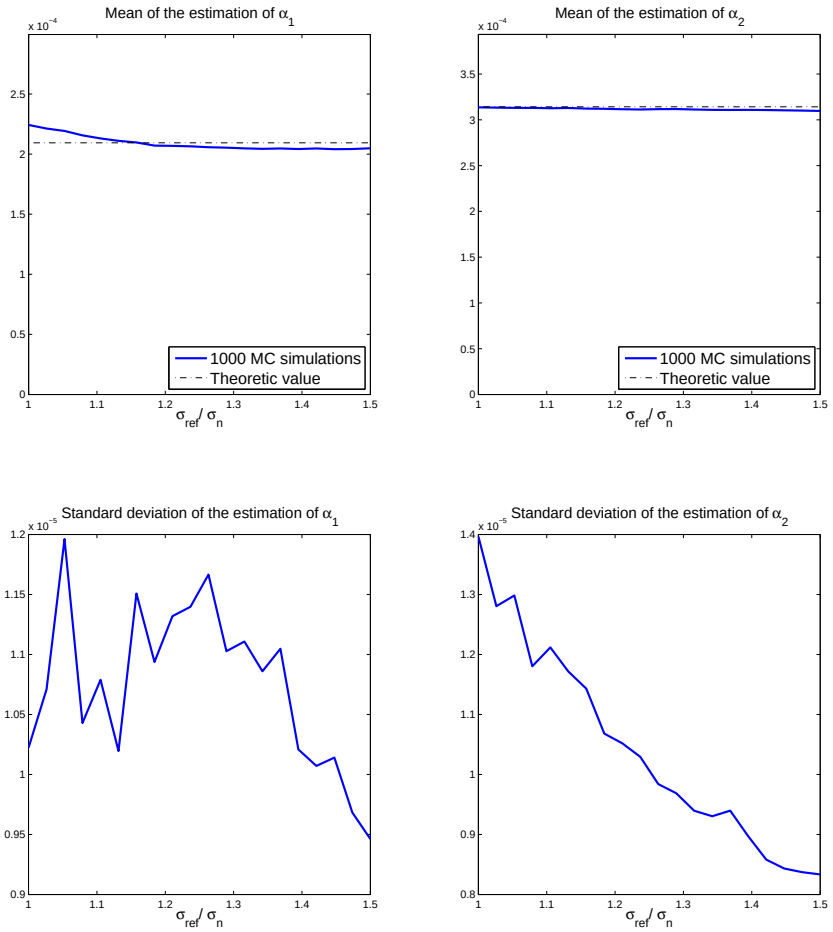

FIGURE 11. Mean and standard deviation of the parameter α of the inclusions.

by [38] in another context. We consider the spiked population model $\mathbf{X}$ with $l_j = 1 + \sigma_j^2(\mathbf{A})$ and we introduce the decomposition $\mathbf{X} = \mathbf{Y} + \mathbf{Z}$ as in the previous step. We denote by $\mathbf{Y} = \mathbf{U_Y D_Y V_Y^\dagger}$ the singular value decomposition of $\mathbf{Y}$. We denote by $\mathbf{A} = \mathbf{U_A D_A V_A^\dagger}$ the singular value decomposition of $\mathbf{A}$.

Let us define

$$\widetilde{\mathbf{B}} = \mathbf{D_A} + \frac{1}{\sqrt{M}} \mathbf{U_Y^\dagger Z V_Y}.$$

We have

$$\mathbf{U_A} \widetilde{\mathbf{B}} \mathbf{V_A^\dagger} = \mathbf{A} + \frac{1}{\sqrt{M}} \mathbf{U_A U_Y^\dagger Z V_Y V_A^\dagger}.$$

Since $\mathbf{U_A U_Y^\dagger Z V_Y V_A^\dagger}$ has the same statistical distribution as $\mathbf{W}$ (the distribution of $\mathbf{W}$ is invariant with respect to multiplication by unitary matrices) and $\widetilde{\mathbf{B}}$ and $\mathbf{U_A}\widetilde{\mathbf{B}}\mathbf{V_A^\dagger}$ have the same singular values, it is sufficient to show the lemma for $\widetilde{\mathbf{B}}$ instead of $\mathbf{B}$.

We have

$$\begin{aligned}\sum_{j=1}^{M\wedge N}\left|\lambda_j\left(\mathbf{S_X}\right)^{\frac{1}{2}}-\sigma_j(\widetilde{\mathbf{B}})\right|^2 &= \sum_{j=1}^{M\wedge N}\left|\sigma_j\left(\frac{1}{\sqrt{M}}\mathbf{X}\right)-\sigma_j(\widetilde{\mathbf{B}})\right|^2\\ &= \sum_{j=1}^{M\wedge N}\left|\sigma_j\left(\frac{1}{\sqrt{M}}\mathbf{U_Y^\dagger X V_Y}\right)-\sigma_j(\widetilde{\mathbf{B}})\right|^2.\end{aligned}$$

Therefore,

$$\begin{aligned}&\sum_{j=1}^{M\wedge N}\left|\lambda_j\left(\mathbf{S_X}\right)^{\frac{1}{2}}-\sigma_j(\widetilde{\mathbf{B}})\right|^2\\ &\le \left\|\frac{1}{\sqrt{M}}\mathbf{U_Y^\dagger X V_Y}-\widetilde{\mathbf{B}}\right\|_F^2 \quad \text{by Lemma C.1}\\ &= \left\|\frac{1}{\sqrt{M}}\mathbf{U_Y^\dagger Y V_Y}+\frac{1}{\sqrt{M}}\mathbf{U_Y^\dagger Z V_Y}-\mathbf{D_A}-\frac{1}{\sqrt{M}}\mathbf{U_Y^\dagger Z V_Y}\right\|_F^2\\ &= \left\|\frac{1}{\sqrt{M}}\mathbf{D_Y}-\mathbf{D_A}\right\|_F^2\\ &= \sum_{j=1}^{M\wedge N}\left|\sigma_j\left(\frac{1}{\sqrt{M}}\mathbf{D_Y}\right)-\sigma_j(\mathbf{D_A})\right|^2\\ &= \sum_{j=1}^{M\wedge N}\left|\sigma_j\left(\frac{1}{\sqrt{M}}\mathbf{Y}\right)-\sigma_j(\mathbf{A})\right|^2\\ &= \sum_{j=1}^{r}\left|\sigma_j\left(\frac{1}{\sqrt{M}}\mathbf{Y}\right)-\sqrt{l_j-1}\right|^2\\ &\overset{M\to\infty}{\longrightarrow} 0 \quad \text{by (35)}.\end{aligned}$$

Therefore, for all $j=1,\dots,r$, we have $\left|\lambda_j\left(\mathbf{S_X}\right)^{\frac{1}{2}}-\sigma_j(\widetilde{\mathbf{B}})\right|^2\to 0$ as $M\to\infty$. Lemma A.1 gives the convergence of $\lambda_j\left(\mathbf{S_X}\right)$, which in turn ensures the convergence of $\sigma_j(\widetilde{\mathbf{B}})$, which completes the proof of Lemma A.2. □

Step 3. Let $\mathbf{A}$ be an $N\times M$ rank-r deterministic matrix whose nonzero singular values are $\sigma_1(\mathbf{A})\ge\cdots\ge\sigma_r(\mathbf{A})>0$. Let $\mathbf{W}$ be an $N\times M$ random matrix with independent and identically distributed complex entries with Gaussian statistics, mean zero and variance σ_{noise}^2. We define

$$\mathbf{B}=\mathbf{A}+\frac{1}{\sqrt{M}}\mathbf{W}.$$

We can now prove the statement of Theorem 2.1.

Proof. We introduce

$$\widetilde{\mathbf{B}}=\frac{1}{\sigma_{\text{noise}}}\mathbf{B},\qquad \widetilde{\mathbf{A}}=\frac{1}{\sigma_{\text{noise}}}\mathbf{A},\qquad \widetilde{\mathbf{W}}=\frac{1}{\sigma_{\text{noise}}}\mathbf{W}.$$

We have

$$\widetilde{\mathbf{B}} = \widetilde{\mathbf{A}} + \frac{1}{\sqrt{M}}\widetilde{\mathbf{W}},$$

where $\widetilde{\mathbf{A}}$ is an $N \times M$ rank-r deterministic matrix whose nonzero singular values are $\sigma_j(\widetilde{\mathbf{A}}) = \sigma_j(\mathbf{A})/\sigma_{\text{noise}}$ and $\widetilde{\mathbf{W}}$ is an $N \times M$ random matrix with independent and identically distributed complex entries with Gaussian statistics, mean zero and variance one. Using Lemma A.2 gives the limits of the singular values of $\widetilde{\mathbf{B}}$, which in turn yields the desired result since $\sigma_j(\mathbf{B}) = \sigma_{\text{noise}}\sigma_j(\widetilde{\mathbf{B}})$. □

Appendix B. **Proof of Theorem 3.1.** We use the same notation as in Appendix A. We address only the case of the left singular vectors, since the result obtained for them can be used to obtain the equivalent result for the right singular vectors after transposition of the matrices.

Step 1. The statistical behavior of the eigenvectors $\boldsymbol{u}_j(\mathbf{S_X})$, $j = 1, \dots, N$ has been obtained in [23] when $l_1 > \cdots > l_r > 1$, $\gamma = N/M$ is fixed and $M \to \infty$:

Lemma B.1. *When $\gamma = N/M$ is fixed and $M \to \infty$ we have for $j = 1, \dots, r$:*

$$\left|\boldsymbol{u}_j(\mathbf{S_X})^\dagger \boldsymbol{u}_j(\mathbf{\Sigma})\right|^2 \overset{M\to\infty}{\longrightarrow} \begin{cases} \dfrac{1 - \frac{\gamma}{(l_j-1)^2}}{1 + \frac{\gamma}{l_j - 1}} & \text{if } l_j > 1 + \gamma^{\frac{1}{2}}, \\ 0 & \text{if } l_j \le 1 + \gamma^{\frac{1}{2}}, \end{cases}$$

almost surely, and for $j \neq k$

$$\left|\boldsymbol{u}_j(\mathbf{S_X})^\dagger \boldsymbol{u}_k(\mathbf{\Sigma})\right|^2 \overset{M\to\infty}{\longrightarrow} 0,$$

in probability.

Here $\mathbf{\Sigma}$ is diagonal with distinct eigenvalues so that the jth singular vector $\boldsymbol{u}_j(\mathbf{\Sigma})$ is the vector $\boldsymbol{e}^{(N,j)}$, that is, the N-dimensional vector whose entries are zero but the j-th entry which is equal to one ($e_k^{(N,j)} = 0$ if $k \neq j$ and $e_j^{(N,j)} = 1$). In fact, this result is proved in [37] in the case of real-valued spiked covariance matrices and it has been recently extended to the complex case in [23].

As shown in Appendix A, we have $\widetilde{\mathbf{S}}_{\widetilde{\mathbf{Y}}} \overset{M\to\infty}{\longrightarrow} \widetilde{\mathbf{\Sigma}}$ almost surely. Since the j-th eigenvector of $\widetilde{\mathbf{\Sigma}}$ is the vector $\boldsymbol{e}^{(r,j)}$, we have by Lemma C.2

$$\left|\boldsymbol{u}_j(\widetilde{\mathbf{S}}_{\widetilde{\mathbf{Y}}})^\dagger \boldsymbol{e}^{(r,j)}\right|^2 \overset{M\to\infty}{\longrightarrow} 1,$$

for all $j = 1, \dots, r$ almost surely. We have

$$\boldsymbol{u}_j(\mathbf{Y}) = \boldsymbol{u}_j\Big(\frac{1}{\sqrt{M}}\mathbf{Y}\Big) = \boldsymbol{u}_j\Big(\frac{1}{M}\mathbf{Y}\mathbf{Y}^\dagger\Big) = \boldsymbol{u}_j(\mathbf{S_Y})$$

and $\boldsymbol{u}_j(\mathbf{S_Y})^\dagger \boldsymbol{e}^{(N,j)} = \boldsymbol{u}_j(\widetilde{\mathbf{S}}_{\widetilde{\mathbf{Y}}})^\dagger \boldsymbol{e}^{(r,j)}$ for all $j = 1, \dots, r$. Therefore

$$\left|\boldsymbol{u}_j(\mathbf{Y})^\dagger \boldsymbol{e}^{(N,j)}\right|^2 \overset{M\to\infty}{\longrightarrow} 1, \tag{37}$$

for all $j = 1, \dots, r$ almost surely.

Step 2. Let $\mathbf{A}$ be an $N \times M$ rank-r deterministic matrix whose nonzero singular values are $\sigma_1(\mathbf{A}) > \cdots > \sigma_r(\mathbf{A}) > 0$. Let $\mathbf{W}$ be an $N \times M$ random matrix with independent and identically distributed complex entries with Gaussian statistics, mean zero and variance one. We define as in Appendix A

$$\mathbf{B} = \mathbf{A} + \frac{1}{\sqrt{M}}\mathbf{W}.$$

Lemma B.2. *When $\gamma = N/M$ is fixed and $M \to \infty$, for any $j = 1, \dots, r$ such that $l_j > 1 + \gamma^{\frac{1}{2}}$ and for any $k = 1, \dots, r$, we have*

$$\left|\boldsymbol{u}_j(\mathbf{B})^\dagger \boldsymbol{u}_k(\mathbf{A})\right|^2 \overset{M\to\infty}{\longrightarrow} \begin{cases} 1 - \frac{\gamma}{(l_j-1)^2} \\ \hline 1 + \frac{\gamma}{l_j - 1} & \text{if } k = j, \\ 0 & \text{otherwise}, \end{cases}$$

in probability, with $l_j = 1 + \sigma_j(\mathbf{A})^2$.

Proof. We use the same notation as in the proof of Lemma A.2. We use again the relationship between randomly perturbed low-rank matrices and spiked population models [38]. Let us fix an index $j = 1, \dots, r$ such that $l_j > 1 + \gamma^{\frac{1}{2}}$. For $k = 1, \dots, r$, let us denote $L_k = \left(l_k + \frac{\gamma l_k}{l_k - 1}\right)^{\frac{1}{2}}$ if $l_k > 1 + \gamma^{\frac{1}{2}}$ and $L_k = 1 + \gamma^{\frac{1}{2}}$ if $l_k \leq 1 + \gamma^{\frac{1}{2}}$. We can find $\delta > 0$ such that $L_j > 2\delta$ and $\min_{k=1,\dots,r,\, k\neq j} \left|L_k - L_j\right| > 2\delta$. We know from Appendix A that $(\sigma_k(\widetilde{\mathbf{B}}))_{k=1,\dots,r}$ and $(\sigma_k(\frac{1}{\sqrt{M}}\mathbf{U}_\mathbf{Y}^\dagger \mathbf{X}\mathbf{V}_\mathbf{Y}))_{k=1,\dots,r}$ both converge to $(L_k)_{k=1,\dots,r}$ almost surely. Therefore, for M large enough, we have

$$\min_{k\neq j} \left|\sigma_j(\widetilde{\mathbf{B}}) - \sigma_k(\frac{1}{\sqrt{M}}\mathbf{U}_\mathbf{Y}^\dagger \mathbf{X}\mathbf{V}_\mathbf{Y})\right| \geq \delta \quad \text{and} \quad \sigma_j(\widetilde{\mathbf{B}}) \geq \delta,$$

and we can apply Lemma C.2 which gives, for M large enough

$$\left|\boldsymbol{u}_j(\widetilde{\mathbf{B}})^\dagger \boldsymbol{u}_j(\frac{1}{\sqrt{M}}\mathbf{U}_\mathbf{Y}^\dagger \mathbf{X}\mathbf{V}_\mathbf{Y})\right|^2 \geq 1 - \frac{2\|\frac{1}{\sqrt{M}}\mathbf{U}_\mathbf{Y}^\dagger \mathbf{X}\mathbf{V}_\mathbf{Y} - \widetilde{\mathbf{B}}\|_F^2}{\delta^2}.$$

Using Appendix A we find that the right-hand side converges almost surely to one, and therefore,

$$\left|\boldsymbol{u}_j(\widetilde{\mathbf{B}})^\dagger \boldsymbol{u}_j(\frac{1}{\sqrt{M}}\mathbf{U}_\mathbf{Y}^\dagger \mathbf{X}\mathbf{V}_\mathbf{Y})\right|^2 \overset{M\to\infty}{\longrightarrow} 1, \tag{38}$$

almost surely. The left singular vectors of $\frac{1}{\sqrt{M}}\mathbf{U}_\mathbf{Y}^\dagger \mathbf{X}\mathbf{V}_\mathbf{Y}$ are related to those of $\mathbf{X}$ through

$$\boldsymbol{u}_j(\frac{1}{\sqrt{M}}\mathbf{U}_\mathbf{Y}^\dagger \mathbf{X}\mathbf{V}_\mathbf{Y}) = \mathbf{U}_\mathbf{Y}^\dagger \boldsymbol{u}_j(\mathbf{X}),$$

and therefore (38) implies

$$\left|\boldsymbol{u}_j(\widetilde{\mathbf{B}})^\dagger \mathbf{U}_\mathbf{Y}^\dagger \boldsymbol{u}_j(\mathbf{X})\right|^2 \overset{M\to\infty}{\longrightarrow} 1, \tag{39}$$

almost surely.

By Lemma B.1 and the fact that $\boldsymbol{u}_j(\mathbf{S}_\mathbf{X}) = \boldsymbol{u}_j(\frac{1}{M}\mathbf{X}\mathbf{X}^\dagger) = \boldsymbol{u}_j(\mathbf{X})$ we have

$$\left|\boldsymbol{u}_j(\mathbf{X})^\dagger \boldsymbol{e}^{(N,k)}\right|^2 \overset{M\to\infty}{\longrightarrow} \xi_j \delta_{jk}, \tag{40}$$

for all $k = 1, \dots, r$ in probability, where $\xi_j = (1 - \frac{\gamma}{(l_j-1)^2})/(1 + \frac{\gamma}{l_j - 1})$. The matrix $\mathbf{U}_\mathbf{Y}$ consists of the left singular vectors of $\mathbf{Y}$ and we have $\mathbf{U}_\mathbf{Y}\boldsymbol{e}^{(N,k)} = \boldsymbol{u}_k(\mathbf{Y})$. By (37) (in Step 1) we find that

$$\left|\boldsymbol{e}^{(N,k)^\dagger}\mathbf{U}_\mathbf{Y}\boldsymbol{e}^{(N,k)}\right| = \left|\boldsymbol{u}_k(\mathbf{Y})^\dagger \boldsymbol{e}^{(N,k)}\right| \overset{M\to\infty}{\longrightarrow} 1, \tag{41}$$

for all $k = 1, \dots, r$. Combining (40) and (41) we obtain

$$\left|[\mathbf{U}_\mathbf{Y}^\dagger \boldsymbol{u}_j(\mathbf{X})]^\dagger \boldsymbol{e}^{(N,k)}\right|^2 = \left|\boldsymbol{u}_j(\mathbf{X})^\dagger \mathbf{U}_\mathbf{Y}\boldsymbol{e}^{(N,k)}\right|^2 \overset{M\to\infty}{\longrightarrow} \delta_{jk}\xi_j,$$

for all $k = 1, \dots, r$ in probability. Using (39) we obtain

$$\left|\boldsymbol{u}_j(\widetilde{\mathbf{B}})^\dagger \boldsymbol{e}^{(N,k)}\right|^2 \overset{M\to\infty}{\longrightarrow} \delta_{jk}\xi_j,$$

for all $k = 1, \dots, r$ in probability. The vector $\boldsymbol{e}^{(N,k)}$ is the k-th left singular vector of $\mathbf{D_A}$, so

$$\left|\boldsymbol{u}_j(\widetilde{\mathbf{B}})^\dagger \boldsymbol{u}_k(\mathbf{D_A})\right|^2 \overset{M\to\infty}{\longrightarrow} \delta_{jk}\xi_j, \tag{42}$$

for all $k = 1, \dots, r$ in probability.

Remember that $\widetilde{\mathbf{B}} = \mathbf{D_A} + \frac{1}{\sqrt{M}}\mathbf{U_Y^\dagger Z V_Y}$, so

$$\mathbf{U_A}\widetilde{\mathbf{B}}\mathbf{V_A^\dagger} = \mathbf{A} + \frac{1}{\sqrt{M}}\mathbf{U_A U_Y^\dagger Z V_Y V_A^\dagger},$$

and $\mathbf{U_A U_Y^\dagger Z V_Y V_A^\dagger}$ has the same statistical distribution as $\mathbf{W}$. As a result $\mathbf{B}$ and $\mathbf{U_A}\widetilde{\mathbf{B}}\mathbf{V_A^\dagger}$ have the same statistical distribution. As a consequence

$$\boldsymbol{u}_j(\mathbf{B}) \overset{in\ dist.}{=} \boldsymbol{u}_j(\mathbf{U_A}\widetilde{\mathbf{B}}\mathbf{V_A^\dagger}) = \mathbf{U_A}\boldsymbol{u}_j(\widetilde{\mathbf{B}}),$$

and

$$\begin{aligned}\left|\boldsymbol{u}_j(\mathbf{B})^\dagger \boldsymbol{u}_k(\mathbf{A})\right|^2 \overset{in\ dist.}{=} \left|\boldsymbol{u}_j(\widetilde{\mathbf{B}})^\dagger \mathbf{U_A^\dagger}\boldsymbol{u}_k(\mathbf{A})\right|^2 &= \left|\boldsymbol{u}_j(\widetilde{\mathbf{B}})^\dagger \boldsymbol{u}_k(\mathbf{U_A^\dagger A V_A})\right|^2 \\ &= \left|\boldsymbol{u}_j(\widetilde{\mathbf{B}})^\dagger \boldsymbol{u}_k(\mathbf{D_A})\right|^2,\end{aligned}$$

which converges in probability to $\delta_{jk}\xi_j$ as $M \to \infty$ by (42). □

Step 3. This step is identical to the one of Appendix A.

Appendix C. Two useful lemmas. We first give a classical lemma that we use in the proof of Theorem 2.1. It can be found for instance in [32, p. 448].

Lemma C.1. *Let* $\mathbf{X}$ *and* $\mathbf{Y}$ *be two* $N \times M$ *matrices. Then we have*

$$\sum_{j=1}^{M\wedge N} \left|\sigma_j(\mathbf{X}) - \sigma_j(\mathbf{Y})\right|^2 \le \left\|\mathbf{X} - \mathbf{Y}\right\|_F^2,$$

where

$$\|\mathbf{X}\|_F^2 = \sum_{n=1}^{N}\sum_{m=1}^{M} |X_{mn}|^2 = \sum_{j=1}^{M\wedge N} \sigma_j^2(\mathbf{X})$$

is the Frobenius norm.

We finally give the statement of a second lemma used in the proof of Theorem 3.1. It can be found for instance in [39, Theorem 4] and it comes from a more general result due to Wedin [42].

Lemma C.2. *Let* $\mathbf{X}$ *and* $\mathbf{Y}$ *be two* $N \times M$ *matrices. Let* $j \le M \wedge N$*. If* $\delta > 0$ *is such that*

$$\min_{k\neq j} \left|\sigma_j(\mathbf{Y}) - \sigma_k(\mathbf{X})\right| \ge \delta \quad \text{and} \quad \sigma_j(\mathbf{Y}) \ge \delta,$$

then we have

$$\left|\boldsymbol{u}_j(\mathbf{Y})^\dagger \boldsymbol{u}_j(\mathbf{X})\right|^2 + \left|\boldsymbol{v}_j(\mathbf{Y})^\dagger \boldsymbol{v}_j(\mathbf{X})\right|^2 \ge 2 - \frac{2\|\mathbf{X} - \mathbf{Y}\|_F^2}{\delta^2}.$$

REFERENCES

[1] M. Alam, V. Cevher, J. H. McClellan, G. D. Larson, and W. R. Scott, Jr., Optimal maneuvering of seismic sensors for localization of subsurface targets, *IEEE Trans. Geo. Remote Sensing*, **45** (2007), 1247–1257.

[2] H. Ammari, *An Introduction to Mathematics of Emerging Biomedical Imaging*, Mathematics & Applications, 62, Springer-Verlag, Berlin, 2008.

[3] H. Ammari, P. Calmon and E. Iakovleva, Direct elastic imaging of a small inclusion, *SIAM J. Imaging Sci.*, **1** (2008), 169–187.

[4] H. Ammari, J. Chen, Z. Chen, J. Garnier and D. Volokov, Target detection and characterization from electromagnetic induction data, *J. Math. Pures Appl.*, **101** (2014), 54–75.

[5] H. Ammari, P. Garapon, L. Guadarrama Bustos and H. Kang, Transient anomaly imaging by the acoustic radiation force, *J. Diff. Equat.*, **249** (2010), 1579–1595.

[6] H. Ammari, J. Garnier, H. Kang, M. Lim and K. Sølna, Multistatic imaging of extended targets, *SIAM J. Imag. Sci.*, **5** (2012), 564–600.

[7] H. Ammari, J. Garnier and K. Sølna, A statistical approach to target detection and localization in the presence of noise, *Waves Random Complex Media*, **22** (2012), 40–65.

[8] H. Ammari, J. Garnier and K. Sølna, Limited view resolving power of linearized conductivity imaging from boundary measurements, *SIAM J. Math. Anal.*, **45** (2013), 1704–1722.

[9] H. Ammari, J. Garnier and K. Sølna, Resolution and stability analysis in full-aperture, linearized conductivity and wave imaging, *Proc. Amer. Math. Soc.*, **141** (2013), 3431–3446.

[10] H. Ammari, J. Garnier, H. Kang, W. K. Park and K. Sølna, Imaging schemes for cracks and inclusions, *SIAM J. Appl. Math.*, **71** (2011), 68–91.

[11] H. Ammari, E. Iakovleva and D. Lesselier, A MUSIC algorithm for locating small inclusions buried in a half-space from the scattering amplitude at a fixed frequency, *Multiscale Model. Simul.*, **3** (2005), 597–628.

[12] H. Ammari, E. Iakovleva and D. Lesselier, Two numerical methods for recovering small inclusions from the scattering amplitude at a fixed frequency, *SIAM J. Sci. Comput.*, **27** (2005), 130–158.

[13] H. Ammari, E. Iakovleva, D. Lesselier and G. Perrusson, A MUSIC-type electromagnetic imaging of a collection of small three-dimensional inclusions, *SIAM J. Sci. Comput.*, **29** (2007), 674–709.

[14] H. Ammari and H. Kang, *Reconstruction of Small Inhomogeneities from Boundary Measurements*, Lecture Notes in Mathematics, Vol. 1846, Springer-Verlag, Berlin, 2004.

[15] H. Ammari and H. Kang, *Polarization and Moment Tensors: with Applications to Inverse Problems and Effective Medium Theory*, Applied Mathematical Sciences, 162, Springer-Verlag, New York, 2007.

[16] H. Ammari, H. Kang, E. Kim and J.-Y. Lee, The generalized polarization tensors for resolved imaging. Part II: Shape and electromagnetic parameters reconstruction of an electromagnetic inclusion from multistatic measurements, *Math. Comp.*, **81** (2012), 839–860.

[17] H. Ammari, H. Kang, H. Lee and W. K. Park, Asymptotic imaging of perfectly conducting cracks, *SIAM J. Sci. Comput.*, **32** (2010), 894–922.

[18] A. Aubry and A. Derode, Random matrix theory applied to acoustic backscattering and imaging in complex media, *Phys. Rev. Lett.*, **102** (2009), 084301.

[19] A. Aubry and A. Derode, Singular value distribution of the propagation matrix in random scattering media, *Waves Random Complex Media*, **20** (2010), 333–363.

[20] A. Aubry and A. Derode, Detection and imaging in a random medium: A matrix method to overcome multiple scattering and aberration, *J. Appl. Physics*, **106** (2009), 044903.

[21] J. Baik and J. W. Silverstein, Eigenvalues of large sample covariance matrices of spiked population models, *Journal of Multivariate Analysis*, **97** (2006), 1382–1408.

[22] G. Bao, S. Hou and P. Li, Inverse scattering by a continuation method with initial guesses from a direct imaging algorithm, *J. Comp. Phys.*, **227** (2007), 755–762.

[23] F. Benaych-Georges and R. R. Nadakuditi, The eigenvalues and eigenvectors of finite, low rank perturbations of large random matrices, *Advances in Mathematics*, **227** (2011), 494–521.

[24] J. Byrnes, *Advances in Sensing with Security Applications*, Springer-Verlag, Dordrecht, 2006.

[25] D. H. Chambers, Target characterization using time-reversal symmetry of wave propagation, *Int. J. Modern Phys. B*, **21** (2007), 3511–3555.

[26] D. H. Chambers and J. G. Berryman, Analysis of the time-reversal operator for a small spherical scatterer in an electromagnetic field, *IEEE Trans. Antennas Propagat.*, **52** (2004), 1729–1738.
[27] D. H. Chambers and J. G. Berryman, Time-reversal analysis for scatterer characterization, *Phys. Rev. Lett.*, **92** (2004), 023902.
[28] A. J. Devaney, Time reversal imaging of obscured targets from multistatic data, *IEEE Trans. Antennas Propagat.*, **523** (2005), 1600–1610.
[29] A. J. Devaney, E. A. Marengo and F. K. Gruber, Time-reversal-based imaging and inverse scattering of multiply scattering point targets, *J. Acoust. Soc. Am.*, **118** (2005), 3129–3138.
[30] J. Garnier, Use of random matrix theory for target detection, localization, and reconstruction, in *Proceedings of the Conference Mathematical and Statistical Methods for Imaging*, (eds. H. Ammari, J. Garnier, H. Kang and K. Sølna), Contemporary Mathematics Series, American Mathematical Society, **548** (2011), 151–163.
[31] D. J. Hansen and M. S. Vogelius, High frequency perturbation formulas for the effect of small inhomogeneities, *J. Phys.: Conf. Ser.*, **135** (2008), 012106.
[32] R. A. Horn and C. R. Johnson, *Matrix Analysis*, Cambridge University Press, Cambridge, 1985.
[33] I. M. Johnstone, On the distribution of the largest eigenvalue in principal components analysis, *Ann. Statist.*, **29** (2001), 295–327.
[34] S. Lee, F. Zou and F. A. Wright, Convergence and prediction of principal component scores in high-dimensional settings, *Ann. Stat.*, **38** (2010), 3605–3629.
[35] J. G. Minonzio, D. Clorennec, A. Aubry, T. Folégot, T. Pélican, C. Prada, J. de Rosny and M. Fink, Application of the DORT method to the detection and characterization of two targets in a shallow water wave-guide, *IEEE Oceans 2005 Eur.*, **2** (2005), 1001–1006.
[36] M. Oristaglio and H. Blok, *Wavefield Imaging and Inversion in Electromagnetics and Acoustics*, Cambridge University Press, 2004.
[37] D. Paul, Asymptotics of sample eigenstructure for a large dimensional spiked covariance model, *Statist. Sinica*, **17** (2007), 1617–1642.
[38] A. Shabalin and A. Nobel, Reconstruction of a low-rank matrix in the presence of Gaussian noise, *Journal of Multivariate Analysis*, **118** (2013), 67–76.
[39] G. W. Stewart, Perturbation theory for the singular value decomposition, in *SVD and Signal Processing, II: Algorithms, Analysis and Applications*, Elsevier, 1990, pp. 99–109.
[40] M. S. Vogelius and D. Volkov, Asymptotic formulas for perturbations in the electromagnetic fields due to the presence of inhomogeneities, *Math. Model. Numer. Anal.*, **34** (2000), 723–748.
[41] D. Volkov, Numerical methods for locating small dielectric inhomogeneities, *Wave Motion*, **38** (2003), 189–206.
[42] P.-Å. Wedin, Perturbation bounds in connection with singular value decomposition, *BIT Numerical Mathematics*, **12** (1972), 99–111.
[43] X. Yao, G. Bin, X. Luzhou, L. Jian and P. Stoica, Multistatic adaptive microwave imaging for early breast cancer detection, *IEEE Trans. Biomedical Eng.*, **53** (2006), 1647–1657.

Received June 2013; revised January 2014.

E-mail address: habib.ammari@ens.fr
E-mail address: garnier@math.univ-paris-diderot.fr
E-mail address: vjugnon@math.mit.edu